


FULL PAPER

Open Access



# Eruption style transition during the 2017–2018 eruptive activity at the Shinmoedake volcano, Kirishima, Japan: surface phenomena and eruptive products

Fukashi Maeno<sup>1\*</sup> , Sayaka Shohata<sup>2</sup>, Yuki Suzuki<sup>3</sup>, Natsumi Hokanishi<sup>1</sup>, Atsushi Yasuda<sup>1</sup>, Yuya Ikenaga<sup>4</sup>, Takayuki Kaneko<sup>1</sup> and Setsuya Nakada<sup>5</sup>

## Abstract

Recent eruptions of the Shinmoedake volcano, Japan, have provided a valuable opportunity to investigate the transition between explosive and effusive eruptions. In October 2017, phreatic/phreatomagmatic explosions occurred. They were followed in March 2018 by a phase of hybrid activity with simultaneous explosions and lava flows and then a transition to intermittent, Vulcanian-style explosions. Evolution of surface phenomena, temporal variations of whole-rock chemical compositions from representative eruptive material samples, and rock microtextural properties, such as the crystallinity and crystal size distribution of juvenile products, are analyzed to characterize the eruption style transition, the conduit location, and the shallow magma conditions of the volcanic edifice. The 2017–2018 eruptive event is also compared with the preceding 2011 explosive–effusive eruption. The chemical and textural properties of the 2018 products (two types of pumice, ballistically ejected lava blocks, and massive lava) are representative of distinct cooling and magma ascent processes. The initial pumice, erupted during lava dome formation, has a groundmass crystallinity of up to 45% and the highest plagioclase number density of all products ( $1.9 \times 10^6/\text{mm}^3$ ). Conversely, pumice that erupted later has the lowest plagioclase number density ( $1.2 \times 10^5/\text{mm}^3$ ) and the highest nucleation density ( $23/\text{mm}^4$  in natural logarithm). This 2018 pumice is similar to the 2011 subplinian pumice. Therefore, it was likely produced by undegassed magma with a high discharge rate. Ballistics and massive lava in 2018 are comparable to the 2011 Vulcanian ballistics. Conversely, the high plagioclase number density pumice that occurred in 2018 was not observed during the 2011 eruption. Thus, such pumice might be specific to hybrid eruptions defined by small-scale explosions and lava dome formation with low magma discharge. The observed transitions and temporal variations of the activities and eruption style during the 2017–2018 Shinmoedake eruptions were primarily influenced by the ascent rate of andesitic magma and the geological structure beneath the summit crater.

**Keywords** Lava dome, Phreatic, Phreatomagmatic, Effusive, Explosive, Subplinian, Number density, Shinmoedake

\*Correspondence:

Fukashi Maeno

fmaeno@eri.u-tokyo.ac.jp

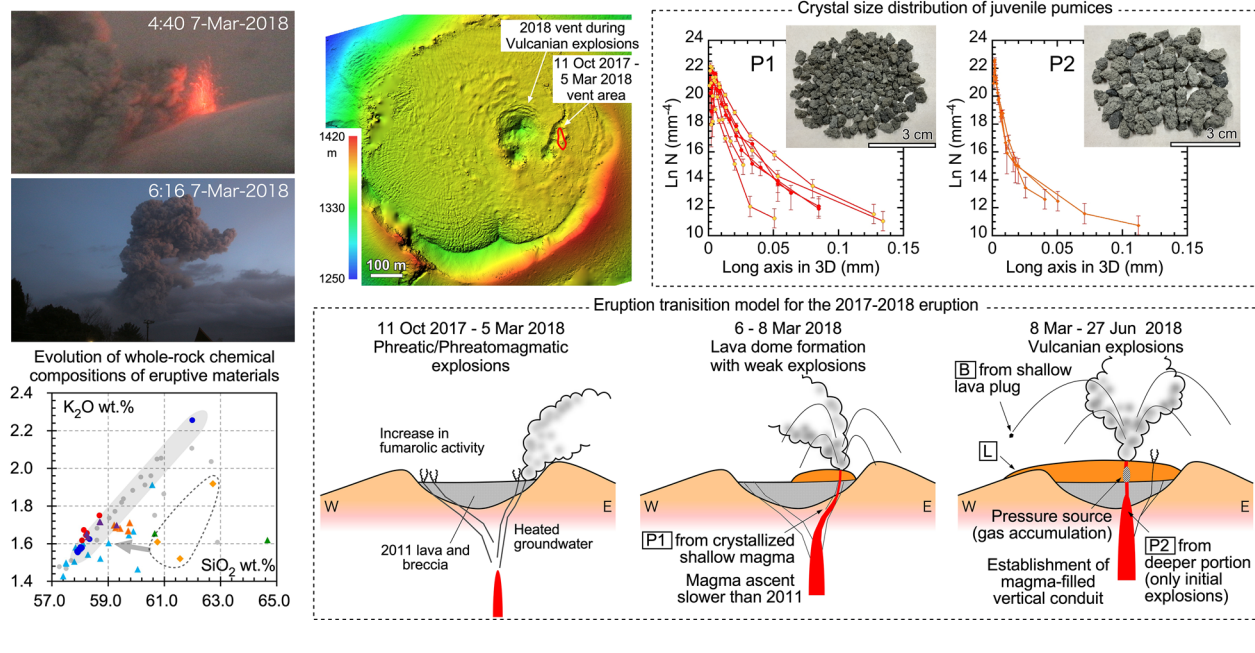
Full list of author information is available at the end of the article



© The Author(s) 2023. **Open Access** This article is licensed under a Creative Commons Attribution 4.0 International License, which permits use, sharing, adaptation, distribution and reproduction in any medium or format, as long as you give appropriate credit to the original author(s) and the source, provide a link to the Creative Commons licence, and indicate if changes were made. The images or other third party material in this article are included in the article's Creative Commons licence, unless indicated otherwise in a credit line to the material. If material is not included in the article's Creative Commons licence and your intended use is not permitted by statutory regulation or exceeds the permitted use, you will need to obtain permission directly from the copyright holder. To view a copy of this licence, visit <http://creativecommons.org/licenses/by/4.0/>.

## Graphical Abstract

## The 2017–2018 explosive-effusive hybrid activity of Shinmoedake volcano, Kirishima, Japan



## Introduction

Andesitic volcanoes exhibit a variety of eruption styles. Even with similar magma compositions, the eruption style can drastically change on a daily to monthly timescale, as seen in recent hazardous eruptive events (Soufriere Hills, Wadge et al. 2014; Merapi, Pallister et al. 2013; Sinabung, Nakada et al. 2019; La Soufriere, Joseph et al. 2022). Variations in eruption style reflect the diversity of magma ascent processes (e.g., Cashman 2004; Gonnermann and Manga 2013). Understanding the causes of such variations is essential to predict transitions in eruption style and associated hazards. Therefore, the geological, geophysical, and theoretical aspects of magma ascent processes, and of their spatial and temporal variations, have been extensively studied (e.g., Cashman and Sparks 2013; Cassidy et al. 2018). The physical and chemical parameters of ascending magmas are key factors in characterizing the ascent process. The textural and chemical characteristics of eruptive products are particularly useful to constrain these magma parameters for shallow conduit ascent and surface emplacement (e.g., Taddeucci et al. 2004; Hammer et al. 1999, 2000; Preece et al. 2013; Mujin and Nakamura 2014; Suzuki et al. 2018).

The recent eruptions of the Shinmoedake volcano in Japan (Fig. 1) provided a valuable opportunity to characterize the transition between explosive and effusive

eruptions. In 2011, the volcano underwent a series of eruptive phases, including three subplinian explosions, the formation of a lava dome, and Vulcanian explosions. The physical and chemical parameters of the ascending magma and the eruption style transitions have been studied in detail (Miyabuchi et al. 2013; Nakada et al. 2013; Kozono et al. 2013; Maeno et al. 2014; Suzuki et al. 2013a, 2013b, 2018; Mujin and Nakamura 2014; Mujin et al. 2017). In 2017–2018, Shinmoedake erupted again after 6 years of dormancy and unrest. The eruption was characterized by phreatic/phreatomagmatic explosions, lava dome growth, and Vulcanian-style eruptions (Fig. 2). It was marked by distinct dynamics relative to the 2011 eruption, which had a subplinian phase, despite the similarity in magma composition (Japan Meteorological Agency 2018). Thus, characterizing the 2017–2018 eruption is important to understand the diversity of andesitic volcano eruptions. However, the characteristics of the eruptive products, surface phenomena, and style transitions of the 2017–2018 eruptions remain poorly constrained, despite the geophysical monitoring summarized by Yamada et al. (2019) and ash textural analyses used to discuss the conduit process that occurred during the 2018 eruption (Matsumoto and Geshi 2021).

In this study, we describe the chronological sequence of surface phenomena that occurred during the 2017–2018 Shinmoedake eruptions, characterize representative

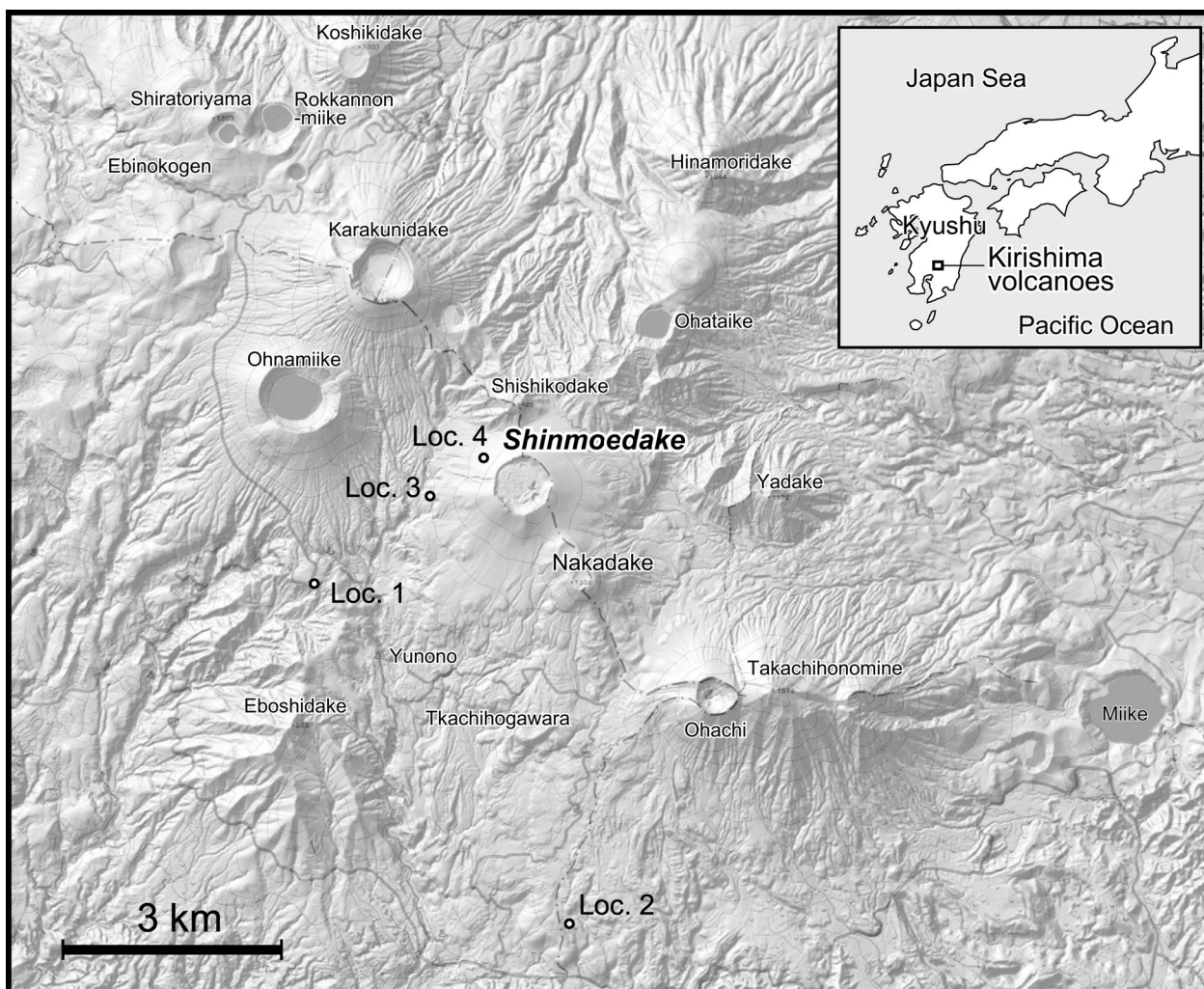


**Fig. 1** Map of Shinmoedake within the Kirishima volcano group and sampling locations (Loc. 1, 2, 3, and 4). The inset shows the position of the Kirishima group in southwestern Japan

ejecta, and compare them with eruptive products from the 2011 eruption. We focus on temporal variations in the bulk ash chemistry and groundmass textures, such as the crystallinity and crystal size distribution (CSD) of juvenile pumice lapilli, ballistics, and lava. The groundmass textures, providing essential information concerning the magma ascent and emplacement processes, are compared with those described in previous studies of the 2011 explosive–effusive eruptions (Suzuki et al. 2013a, 2018). Then, we discuss the causes of the eruption style change during the 2017–2018 eruptions. We use representative samples similar to those analyzed by Matsumoto and Geshi (2021) but propose a more comprehensive eruption model, including a detailed comparison with surface phenomena.

### Geological setting

Shinmoedake (1250 m above sea level) is an active andesitic volcano of the Kirishima volcano group in southern Kyushu, Japan. This volcano group includes more than 20 stratocones and maars (Fig. 1). Activity during the last 1000 years occurred primarily at the Shinmoedake, Ohachi, and Ioyama volcanoes that erupted basaltic and andesitic lava flows and tephra (Imura and Kobayashi 2001). An explosive magmatic eruption and extensive tephra dispersal from Shinmoedake occurred in 1716–1717. The eruptive volume was estimated at approximately 0.2 km<sup>3</sup> (Imura and Kobayashi 1991). Subsequently, smaller eruptions occurred in 1822, 1959, and 1991. The activity at Shinmoedake has recently increased. After a phreatic explosion on 22 August 2008, minor phreatic explosions occurred sporadically on 15

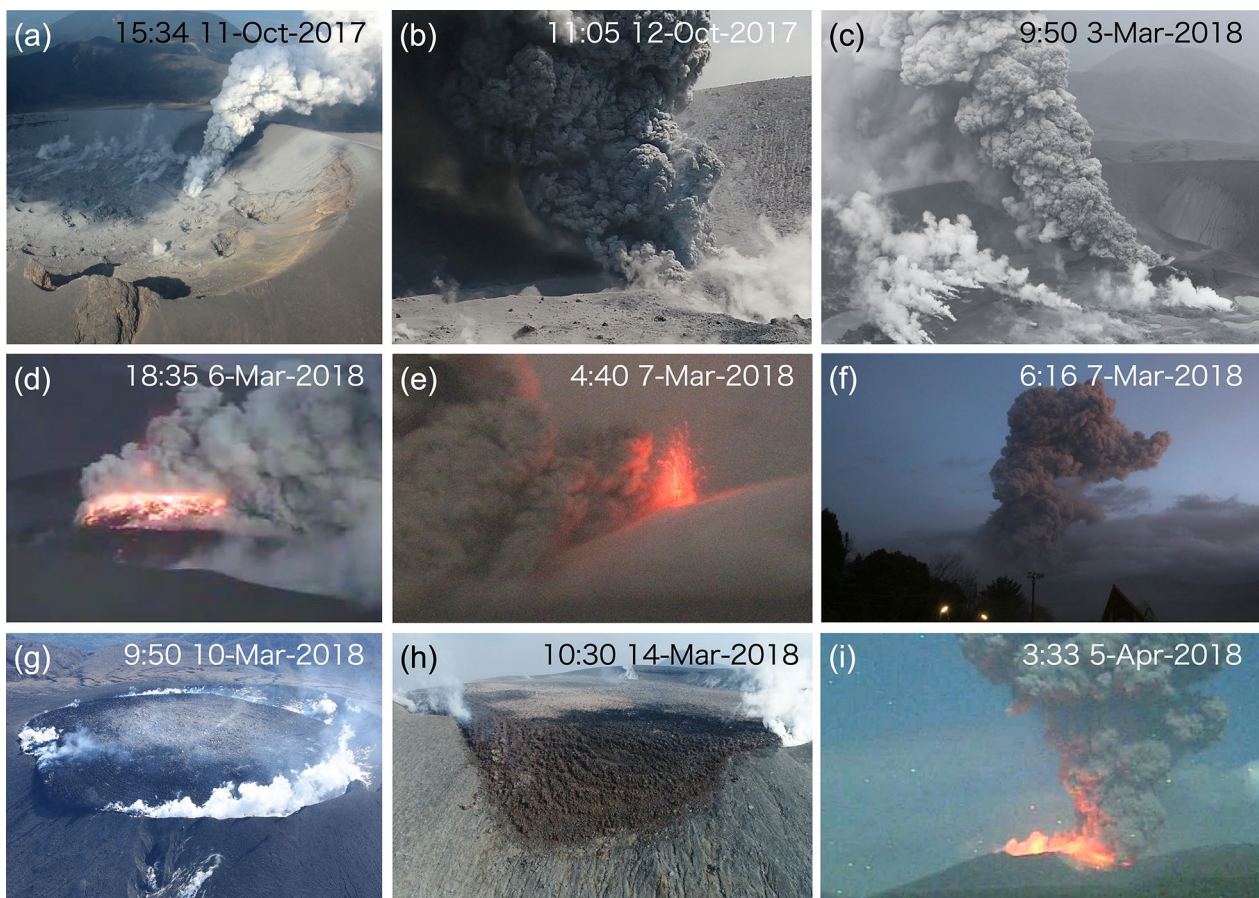


**Fig. 2** Photographs of the 2017–2018 Shinmoedake eruptions. **a** Weak white plume generated by the first eruption (phreatic) from the eastern side of the summit crater on 11 October 2017. **b** Vigorous dark plume on 12 October 2017. **c** Stronger light gray/white plume that developed on 3 March 2018. **d** Lava dome starting to form on the eastern side of the summit crater on 6 March 2018 (credits: JMA). **e** Weakly explosive eruptions associated with lava dome growth observed in the early morning of 7 March 2018. **f** Intense explosion later the same morning. **g** Lava dome nearly overflowing from the northwestern side of the summit crater rim on 10 March 2018. **h** Lobe-shaped lava overflow advancing on the northwestern flank on 14 March 2018. **i** Intense Vulcanian explosion on 5 April 2018 (credits: JMA)

November 2009 and from March to July 2010. These were followed by a larger-scale event in 2011, during which approximately  $0.03 \text{ km}^3$  of magma was erupted by subplinian and Vulcanian explosions and by lava dome formation (Nakada et al. 2013; Kozono et al. 2013; Maeno et al. 2014). Finally, the most recent series of eruptions in 2017–2018 spewed magma and further modified the summit topography.

## Materials and methods

### Observation of surface phenomena

Throughout the 2017–2018 Shinmoedake eruptions, remote observations from airplanes and drones were used to characterize the eruptive dynamics. Airborne observations were conducted on 11 October 2017 and 3, 9–10, and 13 March 2018 onboard a small aircraft from the New Japan Aviation Co., Ltd., and helicopters from the Kagoshima Yomiuri Television and

Miyazaki Telecasting Co., Ltd. Drone observations near the Shinmoedake summit crater and flanks were conducted using DJI Phantom 4 Pro and Inspire 2 standard commercial drones on 12 October 2017 and 14 March, 15–16 April, and 4 June 2018. Remote observation data (from aerial and satellite-borne instruments) from the Japan Meteorological Agency (JMA; Japan Meteorological Agency 2018) and the Geospatial Information Authority of Japan (GSI; Geospatial Information Authority of Japan 2018) were also included in the analysis.

### Rock sampling

Lava blocks, pumice lapilli, and ash samples were collected by the Earthquake Research Institute (ERI) of the University of Tokyo at four locations near and on Shinmoedake during and after the 2017–2018 eruptions (Table 1). Sampling locations and dates are indicated in

Fig. 1 and Table 1, respectively. The methods and instruments are detailed in the following sections. Ash samples from representative explosion events (Fig. 3a–c) were analyzed to determine the temporal variations in the involvement of juvenile and non-juvenile materials using their whole-rock major element compositions, as previously applied to the 2011 event (Suzuki et al. 2013b). Four main juvenile lapilli and lava sample types (hereafter P1, P2, B, and L) were used for chemical and microtextural analyses of the 2017–2018 eruptive process. The deposits from this eruption range from ash fraction to lapilli-sized pumice; however, only lapilli-sized pumice was used because the aim of this study includes measuring the density of pumice lapilli and analyzing the microtexture corresponding to these samples to compare with the previous study (Suzuki et al. 2018). The selected largest clasts were used to measure the bulk density of the pumice. In the microtextural analysis, up to three microscale areas were randomly selected in a single pumice clast to capture the textural heterogeneity. This workflow is not

the same as the standard methodology proposed by, for example, Shea et al. (2010), in which 100 individual lapilli are measured for density and only the ones with median density are selected for further analyses, ensuring representativity. We could not follow this method because the number and size of samples obtained in this study were very limited.

Sample P1 is gray pumice lapilli (diameter: 0.5–1.0 cm; Fig. 3d–f) ejected from small-scale explosions associated with lava dome growth on the night of 6–7 March 2018. Sample P1 was collected at Shinyu (Location 1 (Loc. 1) in Fig. 1), approximately 3 km west of Shinmoedake, the day after the eruption. The four largest pumice clasts were selected for microtextural analysis, while only the largest one, which had sufficient volume, was used for the measurement of the bulk density because the clast size of the deposit from this eruptive phase was generally small. This type of pumice likely corresponds to the “Group A particles” of Matsumoto and Geshi (2021). Sample P2 is light gray pumice lapilli (diameter: 1.3–2 cm; Fig. 3g) also

**Table 1** Lapilli and lava samples from the 2017–2018 magmatic eruptions used in this study

Sample name	Sampling date	Sample type	Location	Eruption date	Origin	Microscope observation	Groundmass and mineral composition analysis	Textural analysis
SNM18_15	7 Mar 2017	Pumice lapilli	P1 Loc. 1	From night on 6 Mar to morning on 7 Mar	Explosion during dome growth	*	*	*
SNM18030708-1	7 Mar 2017	Pumice lapilli	P1 Loc. 1	From night on 6 Mar to morning on 7 Mar	Explosion during dome growth	*		*
SNM18_16	10 Mar 2017	Pumice lapilli	P2 Loc. 2	From night on 8 Mar to 9 Mar	Explosion during dome growth	*	*	*
SNM190305-1–2	5 Mar 2019	Lava block	B Loc. 3	Unknown (after dome formation)	Vulcanian after dome growth	*		*
SNM190305-2	5 Mar 2019	Lava block	B Loc. 3	Unknown (after dome formation)	Vulcanian after dome growth	*	*	*
SNM190420A-1E	20 Apr 2019	Lava	L Loc. 4	From 9 Mar to the end of eruption	Lava overflowed from summit	*		*
SNM19051302-2–22	13 May 2019	Lava	L Loc. 4	From 9 Mar to the end of eruption	Lava overflowed from summit	*		*
SNM19_17	13 May 2019	Lava	L Loc. 4	From 9 Mar to the end of eruption	Lava overflowed from summit	*	*	*

(See figure on next page.)

**Fig. 3** Photographs of representative eruptive products. Top row: volcanic ash from eruptions on (a) 12 October 2017, (b) 14 October 2017, and (c) 5 April 2018. d Ash and pumice lapilli deposit at Loc. 1, approximately 3 km from the Shinmoedake summit crater, on the morning of 7 March 2018. e Magnification of deposit (d) showing abundant pumice lapilli. f Gray pumice collected at Loc. 1. g Light gray pumice erupted on 8–9 March 2018 and collected on 10 March 2018 at Loc. 2. h Ballistic ejecta (lava blocks) that damaged the ground surface and grass at Loc. 3. The inset shows the prismatic jointed surfaces of the blocks. i Tongue-shaped lava overflow from the northwest side of the summit crater. Lava blocks (inset) were sampled from the massive part of the lava flow (Loc. 4)

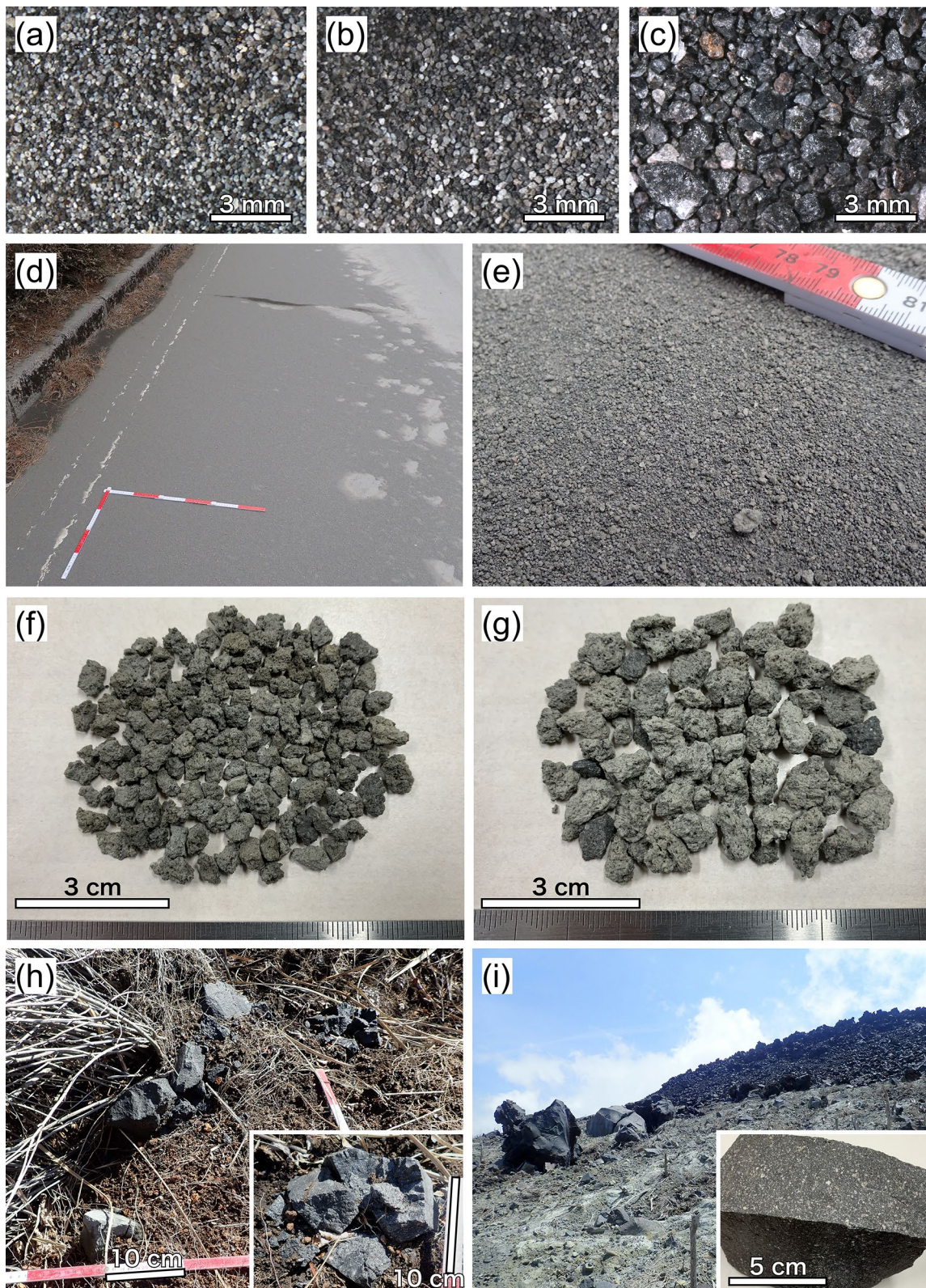


**Fig. 3** (See legend on previous page.)

ejected from explosions during dome growth but collected at the second location (Loc. 2; Fig. 1) on 10 March 2018. Observations of the plume dispersion direction and of the ejecta distribution (The Joint Research Team for ash fall from Shinmoedake 2018) indicate that the eruption that produced P2 likely occurred on 8–9 March 2018; however, the exact eruption time is unknown. We believe that this type of pumice was not included in any of the ash samples analyzed by Matsumoto and Geshi (2021). In the bulk density measurement for Sample P2, the 10 largest clasts that had sufficient volume for the measurement were used, of which one with the average clast density was used for the microtextural analysis. Sample B is a poorly vesiculated lava block (Fig. 3h) ejected ballistically from a Vulcanian explosion during dome growth. It was collected from a new impact crater formed near the ERI seismic station (Loc. 3; Fig. 1), 1.5 km from the summit crater rim, on 5 March 2019, after access restrictions near the summit crater were lifted. This sample likely corresponds to the crystalline, poorly vesiculated “Group B” ash samples of Matsumoto and Geshi (2021). Its eruption date is unknown; however, the block and the new impact crater apparently formed during the 2017–2018 eruptions. Sample L (Fig. 3i) consists of clinker from the lava lobe that outflowed onto the northwestern flank of Shinmoedake. This sample group was collected from the lava lobe front on 20 April and 13 May 2019 (Loc. 4; Fig. 1).

#### Ash component analysis

The ash components were analyzed with a stereomicroscope to obtain the dominant grain size in each sample (125–250  $\mu\text{m}$  grains for the 12 and 14 October 2017 eruptions and 250–500  $\mu\text{m}$  grains for the 8 March and 5 April 2018 eruptions) (Fig. 3a–c) and divided into several types based on their texture, color, and shape: fresh vesiculated particles including pumice and scoria, non-altered and altered lithic, and crystal fragments. Pumice and scoria are colorless and black glassy particles, respectively, with irregular shapes and characterized by the presence of small bubbles. Non-altered lithic is gray, dense, crystalline lava with angular shapes. Contrarily, altered lithic is red/white/yellow, suggesting hydrothermally altered or oxidized, dense, crystalline lava with subangular shapes. Crystal fragments are mainly composed of isolated and almost euhedral crystals, identical in type to phenocrysts.

#### Phenocryst type and mode analysis

The phenocryst types were analyzed with a polarizing microscope for the four samples (P1, P2, B, and L), and the mode composition of phenocrysts with

diameters  $> 200 \mu\text{m}$  was determined by point counting for the lava sample (L).

#### Chemical analyses

The whole-rock major element compositions for the bulk ash, pumice lapilli, and lava blocks were determined at ERI by X-ray fluorescence spectrometry (ZSX Primus II, Rigaku Co., Ltd., Tokyo, Japan). Major chemical compositions of the groundmass glass and mineral phases for the pumice lapilli and lava were also analyzed at ERI using an electron probe microanalyzer (EPMA, JXA-8800R, JEOL Ltd., Tokyo, Japan) with an acceleration voltage of 15 kV, a beam current of 12 nA, and a beam diameter of  $< 10 \mu\text{m}$ . The Na and K contents were measured first to limit losses.

#### Measurement of density

The sample volumes were measured at ERI using three-dimensional (3D) laser scanners (LPX-1200, Roland DG Corporation, and V2, Matter and Form Inc.) with a spatial resolution of 0.1 mm. The bulk densities of the pyroclasts and lavas were calculated from their weights and volumes. The densities of each type of clast were also estimated based on vesicularities measured via microtextural analysis as described below. The density errors were evaluated from both the volume measurements and the vesicularity.

#### Estimation of groundmass crystallinity

The groundmass crystallinity was calculated from the proportion by weight (in wt.%) of potassium oxide ( $\text{K}_2\text{O}$ ) in the crystal and melt phases. If  $B$ ,  $P$ , and  $G$  are the  $\text{K}_2\text{O}$  wt.% in the bulk groundmass, plagioclase microlites, and groundmass glass, respectively, then the groundmass crystallinity ( $C$ ) is expressed as  $C = 100(B - G)/(P - G)$ . Although the groundmass glass and mineral phases were analyzed, it was difficult to analyze the bulk groundmass chemical composition, including both glass and microlites; therefore, the bulk groundmass chemical composition was assumed to be identical to that of the ejecta from the 2011 eruption because the whole-rock chemical composition and the phenocryst types and amounts in our samples were comparable to the 2011 values (Suzuki et al. 2013a). Volatile contents and species were not measured in this study. Plagioclase microlite chemical compositions were assumed to be identical to those of the plagioclase (micro) phenocryst rims because the microlites were markedly smaller than the beam diameter. For each sample, distinct average chemical compositions were assumed for the groundmass glass and for the plagioclase (micro) phenocryst rim.

### Microtextural analysis

Microtextural images of the groundmass in representative samples were acquired at ERI using a field emission EPMA (FE-EPMA, JXA-8530F Plus, JEOL Ltd.) (Fig. 4). For the textural analyses, two element mappings were prepared: (1) 600 pixels per side with a pixel size of 0.2  $\mu\text{m}$  and (2) 800 pixels per side with a pixel size of 0.5  $\mu\text{m}$ . For the microlite analysis, up to three areas were selected randomly and analyzed for each thin section.

Crystal number and size analyses were only conducted for the plagioclase microlites, the main component of the groundmass microlites. In the color-coded images for each mineral type, only plagioclase was masked and analyzed using the public domain processing software “ImageJ” (<https://imagej.nih.gov/ij/>). After noise reduction, the long-axis, short-axis, area, center, and tilt of the plagioclase microlites were measured. For the crystal number and size analysis, we followed the method of Suzuki et al. (2018). Then, stereological corrections

were calculated with the “CSDCorrections” software (Higgins 2000) to reconstruct the 3D crystal size distribution. Input parameters for CSDCorrections included the groundmass area, crystal shape (set to “block”), texture (“massive”), axis used for the two-dimensional size distribution estimation (“width”), and two-dimensional size range. The plagioclase number density was calculated from the reconstructed 3D results. In fact, multiple locations were measured within a single sample, such that the area measured at each location and the corresponding number of crystals were different. In this study, 100–200 crystals were measured in one area, and up to 750 crystals were measured per sample. In addition, crystals touching edges were excluded. The minimum length or area of the crystals used were 1–2  $\mu\text{m}$  or 5–10 pixels, respectively. Although it is recommended to use crystals smaller than 1/10th of the image size when analyzing size distributions (e.g., Shea et al. 2010), the plagioclase microlites analyzed in this study, which used 120  $\mu\text{m}$  or

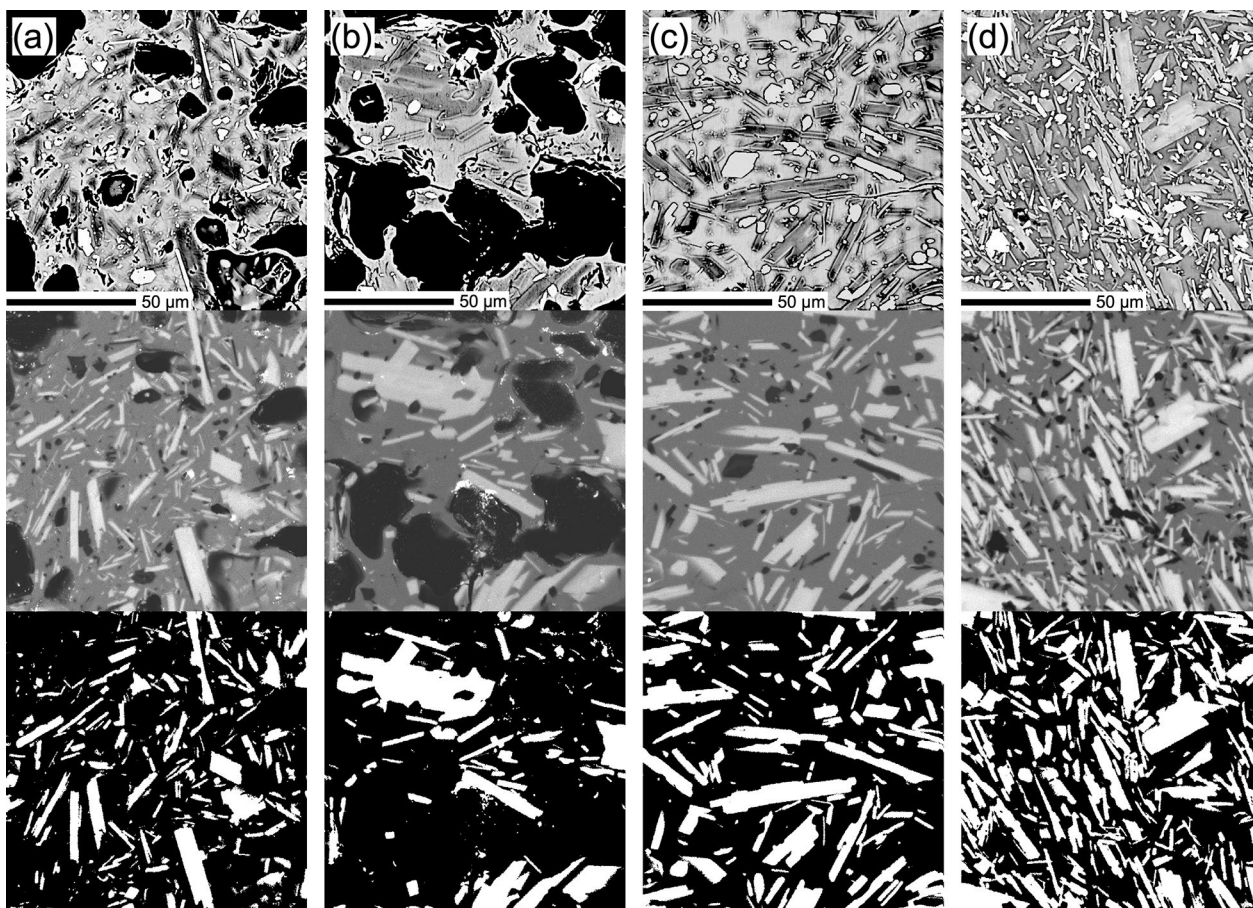


**Fig. 4** Microtextures of rock samples used for textural analyses with images acquired by FE-EPMA. Columns: **a** Sample P1, pumice erupted on 6–7 March 2018 collected at Loc. 1; **b** Sample P2, pumice erupted on 8–9 March 2018 collected at Loc. 2; **c** Sample B, ballistic lava block collected at Loc. 3 on 5 March 2019; and **d** Sample L, massive lava collected from the northwestern flank outflow at Loc. 4. Upper row: backscattered images; middle row: aluminum-phase maps for plagioclase crystals identification; and bottom row: plagioclase-masked images accounting for all elements



400 μm square images, include relatively coarse-grained crystals exceeding several tens of micrometers. Therefore, the discussion deals primarily with crystals smaller than 0.02 mm. When the 2018 crystal number density estimates are compared with the 2011 data (Suzuki et al. 2018), a weighted average value by area was used as the representative crystal number density for crystals with long-axis diameters greater than 0.01 mm for each sample. The vesicularity data were also obtained via ground-mass analyses using 400 μm square images for each sample and were used to estimate the sample density.

**Results**

**Chronology of the 2017–2018 Shinmoedake eruptions**

*The October 2017 phreatic eruption*

Phreatic eruptions started at 05:35 on 11 October 2017 from the eastern side of the summit crater following 6 years of unrest that included shallow seismic activity between 23 September and 9 October 2011 and continuous tremor activity starting on 9 October 2011 (Japan Meteorological Agency 2018). The eruptions were sustained and continued until 16:00 on 13 October 2017. They were initially characterized by a minimum of two plumes generated by several closely grouped small craters on the eastern side of the Shinmoedake summit crater. These plumes soon merged into a larger, single white plume that reached a maximum height of 2.3 km. Relatively weak, the plume bent toward the eastern side on 11 October (Fig. 2a) but subsequently became stronger and turned gray, suggesting an increase in the mass discharge rate and in the fraction of solid particles (Fig. 2b). Phreatic eruptions resumed at 08:23 on

14 October and ended at approximately 00:30 on 17 October. Throughout this eruptive event, fumaroles inside the summit crater became active and generated steam. The October 2017 eruptions generated a small volume of ashfall (on the order of 10<sup>8</sup> kg; Oikawa et al. 2018) around Shinmoedake. Representative ash samples are shown in Fig. 3a–b. Furthermore, these eruptions formed small craters on the eastern edge of the 2011 lava dome that had filled the summit crater (Fig. 5a). This location corresponds to a fumarolic area that existed prior to the 2011 eruption and to a small crater formed in 2011.

*The March–June 2018 eruption*

*Phreatic/phreatomagmatic explosion phase* Phreatic/phreatomagmatic explosions started on the morning of 1 March 2018. Our airborne observation at approximately 09:30 on 3 March 2018 determined that the vigorous gray eruption plume was rising from the same location as in 2017, on the eastern side of the summit crater. The eruption style was similar to that of the 2017 eruption but with a larger vent size and the formation of a small pyroclastic cone (Fig. 2c). The fumaroles inside the summit crater were more active than those in 2017, with vigorous steam generation. These observations suggest that the early March eruption was marked by a higher intensity relative to the 2017 event.

*Dome-forming phase* After the phreatic/phreatomagmatic phase, a lava dome started forming on the eastern vent on 6 March 2018. Lava continuously effused from the

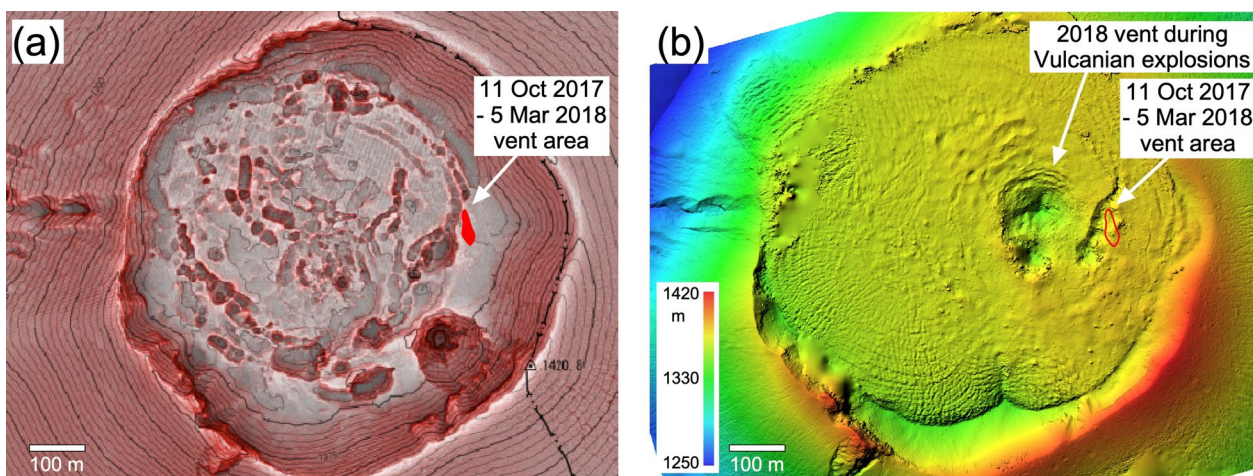


**Fig. 5** Topography of the Shinmoedake summit crater (a) before and (b) after the 2017–2018 eruptions. Major vent locations are indicated. A large fracture zone, formed in 2018 on the eastern surface of the dome, overlaps the vent area of October 2017. The 2018 vent, caused by Vulcanian explosions, is located westward of the 2017 vent area. Map (a) is a Red Relief Image Map made by Asia Air Survey Co., Ltd., from GSI topographic data. Map (b) is derived from photogrammetry from data acquired during our drone survey on 9 February 2019

eastern side of the summit crater, spreading nearly circularly. Intermittent small-scale explosions were associated with lava dome growth, with incandescent ballistics and ash plumes observed at night (Fig. 2e–f). Initially located on the eastern edge of the summit crater, as during the phreatic/phreatomagmatic phase, the lava vent then migrated toward the crater center (Fig. 5b). The temporal evolution of the lava dome was monitored via satellite-borne interferometric synthetic aperture radar (Geospatial Information Authority of Japan 2018). By 00:00 on 8 March, the lava dome had nearly filled the summit crater. Then, the lava supply and dome growth rate declined until 9 March. In the afternoon of 9 March, lava started to overflow from the northwestern rim, at the lowest point of the summit crater rim, and advanced onto the flank (Fig. 2g). Progressing slowly on the flank slope, the lava flowed away from the crater rim by a few tens of meters within a day (9–10 March). Lava further advanced on the northwestern slope until the afternoon of 14 March, forming a tongue-shaped lobe (Fig. 2h). By the end of March 2018, the lobe extended approximately 150 m from the summit crater rim. Fumaroles were particularly active at the western margin of the lava overflow.

**Vulcanian explosion phase** In the afternoon of 8 March, during the major lava effusion phase, a series of frequent Vulcanian-style explosions started at the center of the lava dome and continued even after the decline of the effusion phase. A similar eruptive activity transition, from lava dome growth to Vulcanian explosions, was also observed in 2011. During the 2018 Vulcanian explosion phase, marked surface deformation was observed. Approximately 10 min prior to an explosion at 10:15 on 10 March, a bun-shaped inflation of the central part of the dome, reaching a height of a few meters or more, was observed during an airborne survey simultaneous with weak ash emission at the explosion site. The main Vulcanian eruption occurred immediately after (Earthquake Research Institute Univ. Tokyo 2018). Similar phenomena were also observed on 14 March during a drone survey prior to a discrete explosion. In the morning, the explosion site was slightly depressed, without visible steam plumes (Fig. 6a). However, 3 min (at 15:15) prior to the explosion, the lava dome center inflated locally and multiple fractures formed (Fig. 6b). Gray-brown ash plumes developed from the fractures. The Vulcanian explosion (Fig. 6c) occurred at 15:18 after the drone had left the summit crater. After the explosion, no mound or ash plumes were observed on the lava surface and the explosion site was calm (Fig. 6d).

After late March 2018, Vulcanian explosions occurred more sporadically; however, their intensity remained high. On 5 April, a large Vulcanian explosion occurred

at 03:31 (Fig. 2i). The eruption plume extended higher than 5 km above the summit, and a crater with a diameter of approximately 100 m formed at the center of the lava dome. Pyroclastic density currents were generated toward the western flank. The lava dome surface around the central crater, originally cut by concentric fractures, was heavily covered by ash and blocks. The ash primarily consisted of fresh lava fragments (Fig. 3c). Subsequently, relatively intense Vulcanian explosions, with plume heights of more than 2 km, occurred at 14:44 on 14 May, at 9:09 on 22 June, and at 15:34 on 27 June. After 27 June, no further explosions occurred.

#### Temporal evolution of whole-rock chemical compositions

The whole-rock major element compositions of bulk ash samples from the 2017 eruptions contained 61–63 wt.% of  $\text{SiO}_2$ , differing markedly from the linear chemical compositional trend observed for the Shinmoedake magmatic eruptions until the 2011 eruptions (Fig. 7 and Table 2). Conversely, the chemical compositions of bulk ash samples after 1 March 2018 gradually became comparable to the Shinmoedake magma trend (Figs. 7, 8): pumice and lava from the major dome-forming phase of March 2018 lie on the Shinmoedake magma trend, including the 2011 juvenile products (Table 2). After March 2018, the bulk ash composition variations were not consistent, except for  $\text{MgO}$  and  $\text{Al}_2\text{O}_3$ , which showed small increasing and decreasing trends, respectively, until the Vulcanian explosion of 14 May 2018 (Fig. 8).

#### Physical, chemical, and textural characterization of eruptive products

Microscopic observations revealed that volcanic ash from the 2017 eruptions contained more than 25% altered (red oxidized or silicified) fragments (Figs. 3a–b and 8). During the 2018 eruptions, their proportion decreased while the proportion of fresh lava fragments increased. The proportion of fresh lava and crystal fragments increased from 37.5% and 11.3%, respectively, on 12 October 2017, to 45.7% and 26.5%, respectively, on 14 October 2017 (Fig. 8). Conversely, the proportion of altered lava fragments decreased from 48.8% on 12 October 2017 to 26.8% on 14 October 2017. There was less than 1% of pumice clasts in the October 2017 erupted products; however, this proportion increased markedly in the ash samples from the early March 2018 eruptions, similarly to the fresh lava and crystal fragments (Fig. 3c). The whole-rock chemical compositions reflected the variations in the proportion of altered fragments.

All juvenile products (pumice and lava) from the 2018 eruptions included phenocrysts (smaller than 1 mm) of plagioclase, orthopyroxene, clinopyroxene, olivine, and

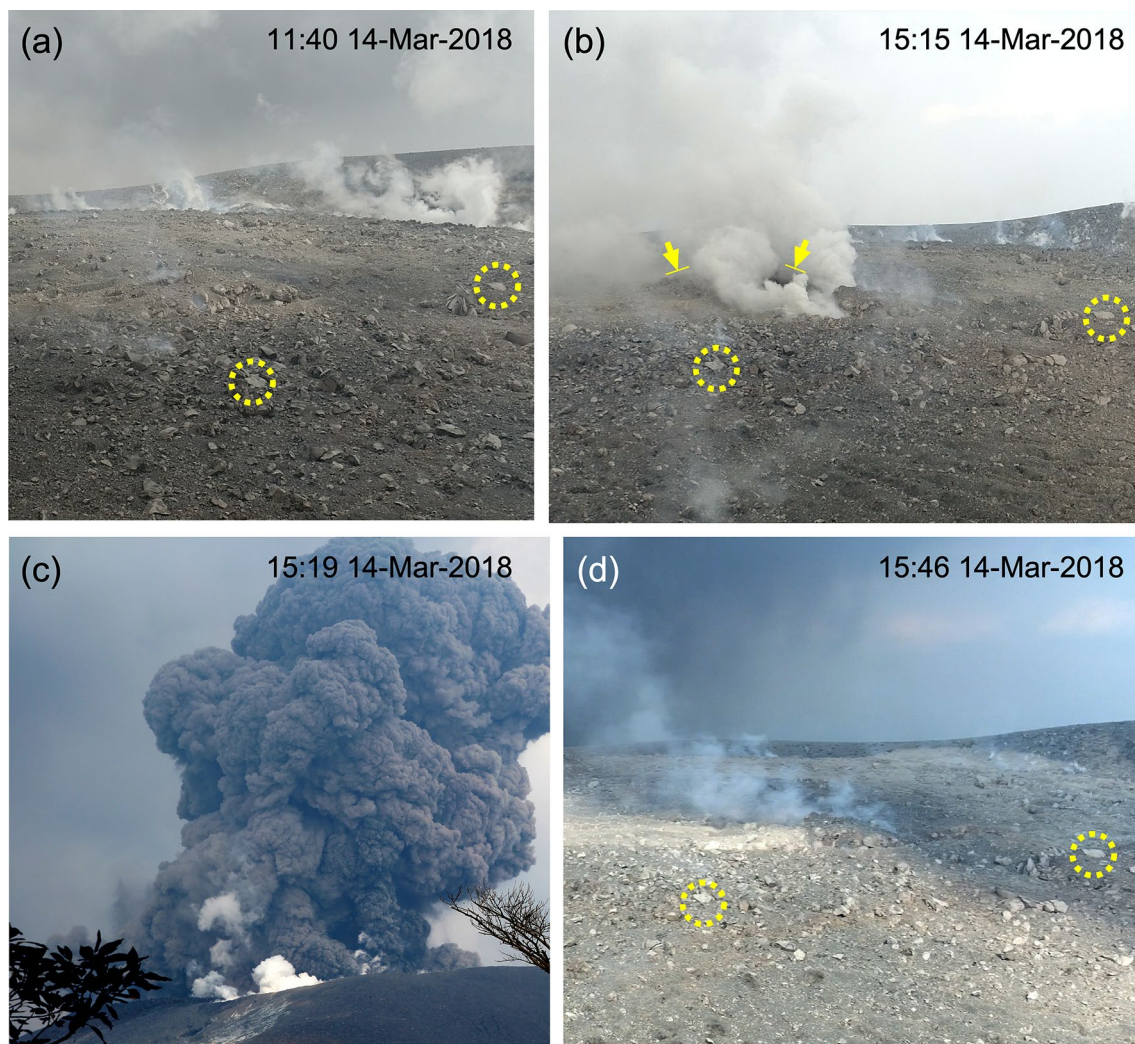


**Fig. 6** Evolution of the Shinmoedake lava dome surface associated with the Vulcanian explosion on 14 March 2018. **a** Lava dome surface more than 3 h prior to the explosion. There was no mound at the dome center in the morning. **b** 3 min prior to the 15:18 Vulcanian explosion, a small mound formed at the future explosion site (yellow arrows) and gas emission increased. **c** Vulcanian explosion viewed from Shinyu (Loc. 1); photograph taken 1 min later (15:19). **d** After the explosion, the mound disappeared and the gas emission decreased. The yellow dotted circles in panels **(a)**, **(b)**, and **(d)** indicate large blocks (scale reference) that were not displaced by the eruption. The approximate distance between the blocks is 100 m

iron–titanium (Fe–Ti) oxides (Table 3). Olivine phenocrysts were less abundant in samples B and L. Some phenocrysts were included as aggregates (glomeroporphyroclasts). The phenocryst types and quantities were nearly identical to those identified in the 2011 eruptive products (Suzuki et al. 2013a).

The estimated sample densities were  $1.3 \text{ g/cm}^3$  for P1,  $1.2 \text{ g/cm}^3$  for P2, and  $2.5\text{--}2.6 \text{ g/cm}^3$  for B and L (Fig. 9). In these estimates including errors, we considered the vesicularities measured through microtexture analyses because of the limited clast volume data available for the bulk density estimation. The vesicularities from the

microtexture analyses were measured at  $42 \pm 3\%$  for P1,  $60 \pm 2\%$  for P2,  $< 1\%$  for B, and  $< 1\%$  for L, which deviates slightly from the vesicularities estimated based on the volume and density data obtained using a 3D laser scanner. These density estimates are similar to those of the 2011 products (Suzuki et al. 2018).

Groundmass glasses were light brown for P1 and P2, brown for B, and black for L. Estimated groundmass crystallinities were  $36.5 \pm 8.6\%$  for P1,  $38.8 \pm 8.6\%$  for P2,  $59.2 \pm 5.6\%$  for L, and  $52.5 \pm 8.0\%$  for B, accounting for the sample chemical characteristics (Fig. 9). The chemical compositions of the groundmass glass and plagioclase

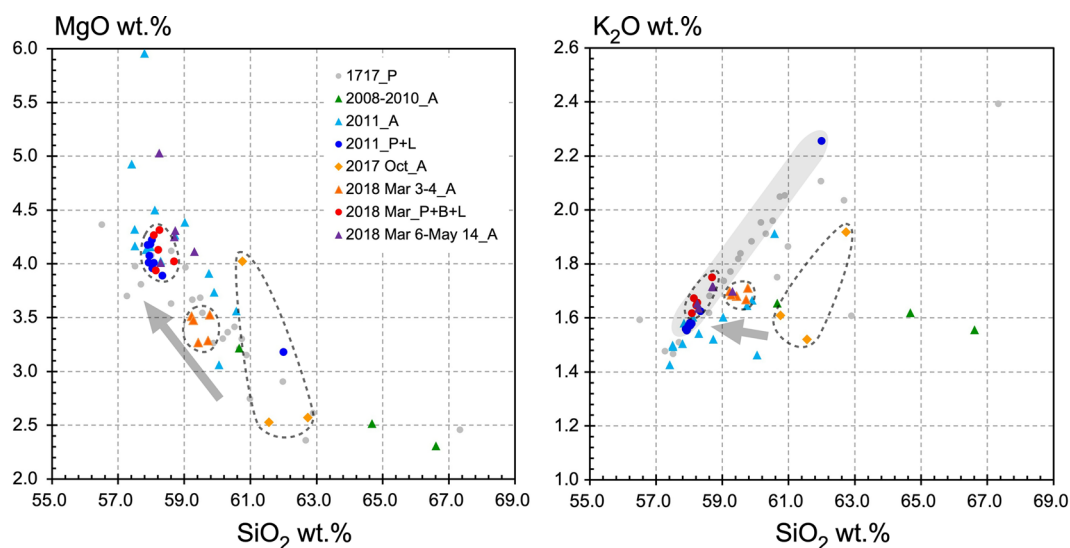


**Fig. 7** Whole-rock chemical compositions of ejecta (*P* pumice, *B* ballistics, *L*: massive lava, and *A* ash) from four Shinmoedake eruptive events: 1717, 2008–2010, 2011, and 2017–2018. Dashed areas indicate bulk ash compositions during specific activity phases in 2017–2018. Arrows indicate bulk ash composition trends, throughout the 2017–2018 event toward the historical Shinmoedake magma composition. The shaded area in the SiO<sub>2</sub>–K<sub>2</sub>O diagram shows the typical magma composition trend since 1717

rim used for the crystallinity estimations are indicated in Table 4. Differences in the estimated groundmass crystallinity were consistent with high-resolution FE-EPMA textural images, which showed that the crystallinity was the highest for Sample L, increased to similar values in Sample B, and was lower for samples P1 and P2 (Fig. 4).

Estimated average plagioclase number densities were  $1.9 \times 10^6/\text{mm}^3$  for P1,  $1.2 \times 10^5/\text{mm}^3$  for P2,  $7.9 \times 10^5/\text{mm}^3$  for L, and  $4.3 \times 10^5/\text{mm}^3$  for B (Fig. 9 and Table 5). The CSD curves for representative samples are shown in Fig. 10 and are compared to estimates for the 2011 eruptive products in Fig. 11. The slope of the CSD curve represents the fraction of crystal growth, with smaller values indicating a predominance of crystal growth over nucleation; the *y*-axis intercept represents the nucleation density, with higher values indicating higher nucleation activity (Cashman 1992; Hammer et al. 1999, 2000). The CSD curves for the 2018 samples are piecewise linear within specific ranges of the crystal 3D long-axis diameter. The *y*-axis intercept (nucleation density) and the slope were determined using data points on the steepest segment smaller than 0.02 mm in the 3D long-axis diameters. The CSD curve for Sample P2 showed the steepest slope (from  $-468$  to  $-669$ ) and the highest *y*-axis intercept value ( $\ln(N_0) = 22.6\text{--}23.3/\text{mm}^4$ ), indicating that small microlites dominate the groundmass texture. The CSD curves for samples P1 and L had similar slopes but were less steep (from  $-152$  to  $-423$ ) than that of P2; their *y*-axis intercepts ( $\ln(N_0) = 21.4\text{--}22.7/\text{mm}^4$ ) were comparable but lower than that of P2. Crystals in samples

L and P1 were larger than those in P2. The CSD slope for Sample B was comparable to those of P1 and L; however, the *y*-axis intercept was lower ( $\ln(N_0) = 20.8\text{--}21.3/\text{mm}^4$ ) and Sample B did not contain large crystals (with 3D long-axis diameters greater than 0.1 mm).

### Discussion

#### Eruption style transition from phreatic/phreatomagmatic to magmatic activity

From October 2017 to early March 2018, eruptions primarily consisted of ash emissions and were considered to be phreatic and phreatomagmatic based on their ash componentry. During this period, prior to the main eruption in March 2018, the whole-rock chemical composition of the volcanic ash showed temporal variations, such as an SiO<sub>2</sub> abundance decrease and an MgO abundance increase (Figs. 7, 8). The ash composition, therefore, became similar to those of the lava and pumice ejected during the main eruption. The deviation of the volcanic ash chemical composition from the essential juvenile material showed contamination by non-juvenile materials, such as altered rock fragments, as confirmed by microscopic observations of the volcanic ash particles. Gradual temporal increases in the essential component abundances in the ash and the inflation of the volcano, represented by the baseline length change (as measured by a global navigation satellite system), prior to the March 2018 eruption (Yamada et al. 2019) indicated that magma was accumulating at a certain depth. The eruptions that occurred from

**Table 2** Whole rock chemical compositions of the eruptive materials during the 2017–2018 Shinmoedake eruption

Sample name	SNM171011-03	SNM171012-02	SNM171014	SNM180303-1	SNM18030301	SNM18030303	SNM18030407	SNM18030411	SNM18030708-ca
Sample type	Ash	Ash	Ash	Ash	Ash	Ash	Ash	Ash	Ash
Abbreviation	A	A	A	A	A	A	A	A	A
Eruption date	11-Oct-17	12-Oct-17	14-Oct-17	3-Mar-18	3-Mar-18	3-Mar-18	4-Mar-18	4-Mar-18	7-Mar-18
SiO <sub>2</sub>	62.73	61.56	60.76	59.42	59.22	59.27	59.77	59.72	58.28
TiO <sub>2</sub>	0.70	0.74	0.72	0.70	0.69	0.70	0.70	0.70	0.63
Al <sub>2</sub> O <sub>3</sub>	17.25	18.60	16.95	17.91	17.70	17.67	17.29	17.63	17.65
tFeO	6.29	7.61	6.72	6.66	6.78	6.85	7.02	7.08	6.85
MnO	0.11	0.09	0.13	0.12	0.13	0.13	0.12	0.12	0.14
MgO	2.57	2.53	4.02	3.27	3.51	3.48	3.52	3.29	4.01
CaO	5.79	5.42	6.52	7.37	7.36	7.37	7.11	7.09	7.83
Na <sub>2</sub> O	2.51	1.81	2.47	2.75	2.79	2.74	2.64	2.60	2.87
K <sub>2</sub> O	1.92	1.52	1.61	1.68	1.70	1.68	1.71	1.67	1.64
P <sub>2</sub> O <sub>5</sub>	0.13	0.13	0.10	0.12	0.12	0.12	0.12	0.12	0.10
Total	100.00	100.00	100.00	100.00	100.00	100.00	100.00	100.00	100.00
Sample name	SNM18030708-p	SNM190305-0102	SNM1903050102	SNM190420A-1	SNM19051301	SNM180320-a	SNM180405-a	SNM180514a	SNM180514c
Sample type	Pumice lapilli	Lava block	Lava block	Lava	Lava	Ash	Ash	Ash	Ash
Abbreviation	P1	B	B	L	L	A	A	A	A
Eruption date	7-Mar-18	23-Mar-18	23-Mar-18	17-Mar-18	17-Mar-18	20-Mar-18	5-Apr-18	14-May-18	14-May-18
		± 14 days	± 14 days	± 8 days	± 8 days				
SiO <sub>2</sub>	58.14	58.69	58.24	58.21	58.07	59.30	58.70	58.24	58.73
TiO <sub>2</sub>	0.68	0.71	0.71	0.72	0.71	0.68	0.70	0.74	0.71
Al <sub>2</sub> O <sub>3</sub>	17.48	16.93	17.03	17.19	17.28	16.97	16.83	15.95	16.66
tFeO	7.12	7.25	7.36	7.31	7.23	7.00	7.34	8.06	7.38
MnO	0.14	0.14	0.14	0.14	0.14	0.14	0.14	0.16	0.15
MgO	3.94	4.02	4.32	4.13	4.27	4.11	4.25	5.03	4.31
CaO	7.81	7.50	7.60	7.67	7.71	7.18	7.38	7.27	7.36
Na <sub>2</sub> O	2.91	2.90	2.82	2.86	2.86	2.80	2.83	2.79	2.88
K <sub>2</sub> O	1.67	1.75	1.66	1.65	1.62	1.70	1.72	1.65	1.72
P <sub>2</sub> O <sub>5</sub>	0.11	0.11	0.11	0.12	0.11	0.10	0.11	0.11	0.11
Total	100.00	100.00	100.00	100.00	100.00	100.00	100.00	100.00	100.00

tFeO total iron as FeO

11 October 2017 to 5 March 2018 were likely caused by the activation or pressurization of a shallow hydrothermal system associated with an input of heat and fluids from the magma accumulation depth. The 2017–2018 volcanic ash composition variations were similar to those recorded at Shinmoedake between the 2008 phreatomagmatic explosion and the January 2011 eruption (Suzuki et al. 2013b), during which the ratio of fresh lava or magma to altered material in the ejecta increased as the eruption proceeded.

In the 2017–2018 activities leading up to the lava effusion event on 6 March 2018, eruptive vents clustered on the eastern margin of the summit crater rather than in its center, where the main vent of the 2011 eruption was located. The distribution of the vents indicates

that outgassing pathways developed on the summit crater margin, likely because the considerable lava outflow of the 2011 eruption had completely filled the original summit crater and effectively acted as a massive plug. Conversely, the boundary between the base of the 2011 lava outflow and the pre-eruptive surface was likely the most porous part of the volcanic edifice, thereby providing active outgassing pathways from a shallow hydrothermal system and/or a slowly ascending and crystallizing magma body and explaining the concentration of small-scale fumarolic activity along the lava dome margin in 2017–2018 (Fig. 12).

On 6 March 2018, lava effusion started on the eastern rim. However, while lava was filling the summit crater and overflowing, explosive eruptions occurred closer to

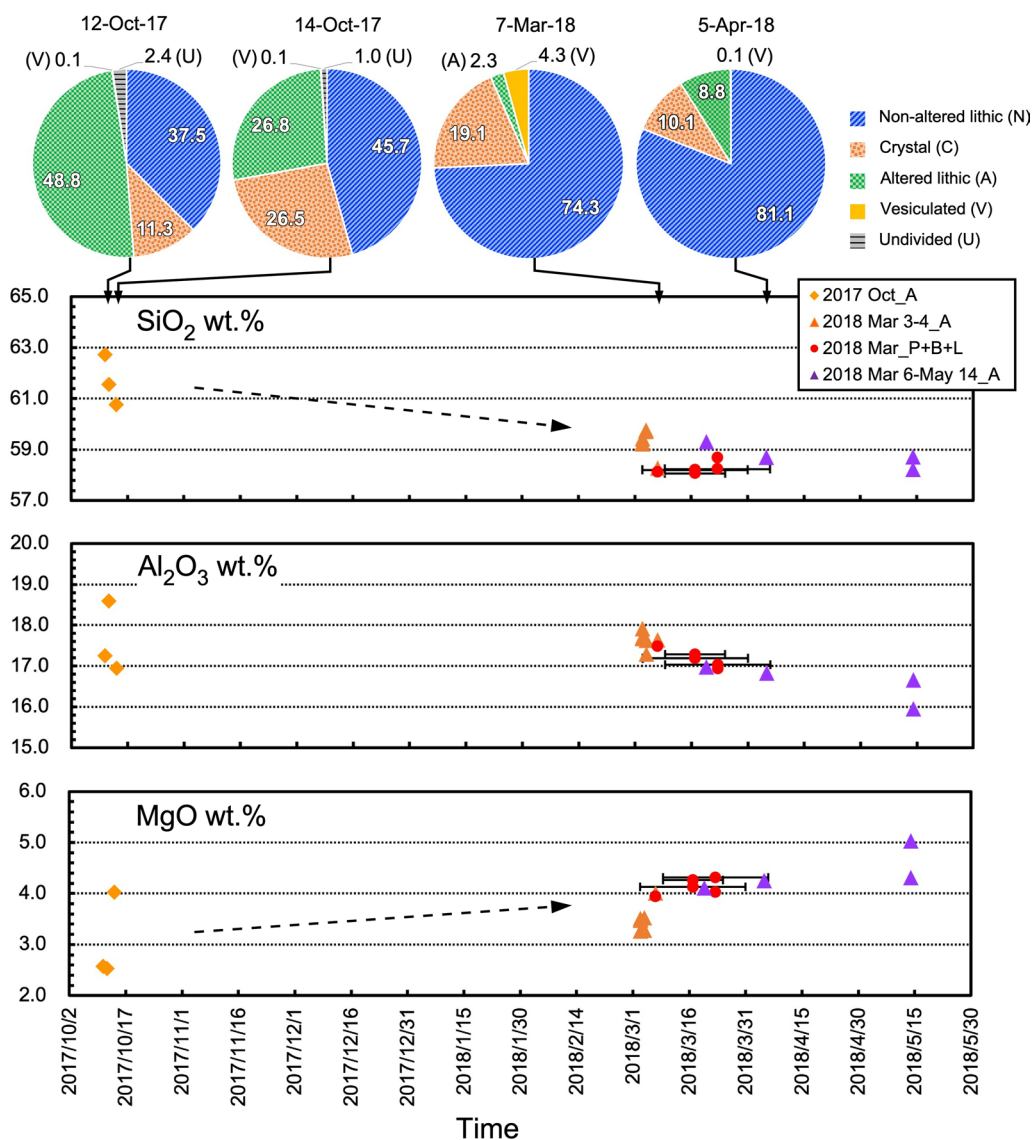


**Fig. 8** Temporal variations in the whole-rock chemical compositions (bottom) and ash components (top) during the 2017–2018 eruptions. Symbols are the same as in Fig. 7

**Table 3** Phenocryst types and contents of the 2018 product

Phenocryst type	2018 lava vol.% <sup>a</sup>	2011 lava <sup>b</sup> vol.%
Plagioclase	25.8	23.0
Orthopyroxene	3.9	3.4
Clinopyroxene	2.6	1.3
Fe-Ti oxides	0.1	1.0
Olivine	0.2	1.3
Phenocryst total	32.6	30.0
Groundmass	67.4	70.0

<sup>a</sup> Based on point counts approximately 2000

<sup>b</sup> Data from Suzuki et al. (2013a)

the center of the new lava dome (Fig. 5), indicating a shift in the magma and outgassing pathway. These observations suggest that the initial bent pathway was replaced by a straight upward pathway into the central crater where the subsequent explosions occurred, likely because of larger magma supply rates (Fig. 12).

Observations of the lava dome surface before and after the Vulcanian eruptions suggest that the inflation source, which may have been caused by the accumulation of gas, was at a shallow depth, although it is difficult to constrain whether a large volume of interconnected gas accumulated at a certain shallow depth or a porous magma just below an impermeable layer in the upper conduit blocked

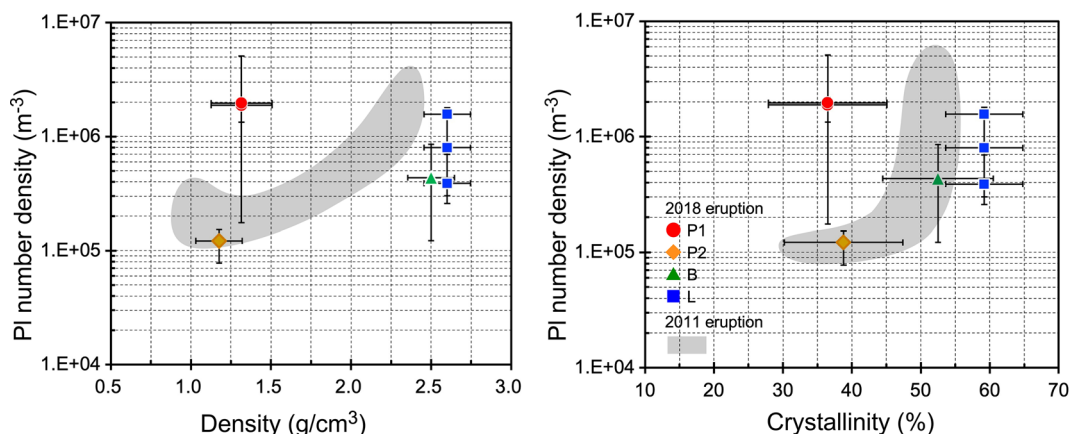


**Fig. 9** Dependence of the density (left) and groundmass crystallinity (right) on the plagioclase number density for representative samples (P1, P2, B, and L) from the 2017–2018 eruptions. For samples P1 and P2, the densities were estimated based on volumes measured using three-dimensional (3D) laser scanners and vesicularities measured via microtextural analyses. The density errors were evaluated from both the volume and vesicularity measurements. The plagioclase number density was calculated only for crystals longer than 0.01 mm. Corresponding results for the 2011 eruption (Suzuki et al. 2018) are indicated by the shaded area in both panels

**Table 4** Groundmass chemical compositions and crystallinity for the representative samples from the Shinmoedake eruptions

Eruption	28 Jan 2011	1 Feb 2011	Mar 2018							
	2011–020503	2011–0201-1	SNM18_15		SNM18_16		SNM190305-2-3		SNM18_17	
Sample name	Pumice	Lava	P1		P2		B		L	
Sample type	Bulk GM	Bulk GM	GM glass	PI rim	GM glass	PI rim	GM glass	PI rim	GM glass	PI rim
SiO <sub>2</sub>	60.87	63.94	68.57	53.26	69.83	53.77	72.63	53.25	76.02	54.35
TiO <sub>2</sub>	0.65	0.65	0.83	0.00	0.65	0.05	0.69	0.11	0.75	0.01
Al <sub>2</sub> O <sub>3</sub>	18.01	16.26	14.19	29.46	14.86	28.45	13.11	28.80	12.48	28.72
tFeO	5.67	5.44	5.17	0.47	3.78	0.94	3.60	1.16	1.88	0.56
MnO	0.12	0.12	0.11	0.00	0.09	0.01	0.07	0.02	0.05	0.01
MgO	2.37	2.11	1.10	0.04	0.69	0.13	0.47	0.15	0.06	0.05
CaO	7.10	5.72	3.68	12.71	3.58	12.54	2.40	13.08	1.01	11.75
Na <sub>2</sub> O	3.19	3.24	2.94	3.76	3.06	3.75	3.06	2.75	2.84	4.23
K <sub>2</sub> O	1.87	2.37	3.18	0.27	3.25	0.34	3.76	0.64	4.74	0.31
P <sub>2</sub> O <sub>5</sub>	0.16	0.16	0.12	0.00	0.11	0.00	0.12	0.00	0.09	0.00
n	480	565	10	3	9	3	6	2	2	3
Crystallinity			36.5 ± 8.6		38.8 ± 8.6		52.5 ± 8.0		59.2 ± 5.6	

outgassing and caused overpressure and inflation. Similarly, analyses of ballistic ejecta from the 2011 Vulcanian eruption also indicated the accumulation of gas in a shallow conduit (50–100 m; Maeno et al. 2013). We believe that shallow inflation sources such as gas accumulation regions and related explosions might be common during lava dome-forming eruptions. The evolution of the crater location and eruptive style during the 2017–2018 eruptions reflects both the shallow edifice structure, including the previous summit crater buried by the 2011 lava, and the higher magma and gas supply rate in 2017–2018 (Fig. 12).

**Explosive–effusive hybrid activity constrained by textural characteristics**

No significant differences were found in the type and chemical composition of phenocrysts from each phase of the March 2018 eruptions. Therefore, we believe that all eruptive activities originated from the same magma reservoir. The vesicularity, crystallinity, crystal (plagioclase) number density, and CSD reflect differences in the magma ascent processes. Variations in the crystallization conditions are recorded as groundmass textural differences. For example, undercooling is recorded as a crystal number density increase (Hammer et al. 1999,

**Table 5** Results of groundmass textural analysis

Type	Sample name	Area no	Conditions in 2D analyses		3D Crystal form Si:L	Number density		CSD y-axis intercept ln(N <sub>0</sub> ) (mm <sup>-4</sup> )	CSD slope
			Reference area (mm <sup>2</sup> )	Count		2D (mm <sup>-2</sup> )	3D (mm <sup>-3</sup> )		
P1	SNM18_15	2	0.0105	137	1:5:5	13,048	2121100	21.9	- 227.7
		4	0.0102	135	1:6.7:6.7	13,235	1336140	22.5	- 260.1
		6	0.0121	233	1:6.7:6.7	19,256	2180160	22.7	- 233.4
P1	SNM18030708-1	5	0.0118	189	1:10:10	16,017	5089880	22.0	- 152.1
		6	0.0118	200	1:6.7:6.7	16,949	1955230	22.6	- 238.6
		7	0.0108	181	1:3.3:3.3	16,759	644400	22.7	- 366.6
		8	0.0116	187	1:6.7:6.7	16,121	175380	21.4	- 331.1
P2	SNM18_16	2	0.0078	94	1:2.5:2.5	12,051	152860	22.6	- 467.7
		3	0.0081	104	1:2.2:2.2	12,840	77,610	23.3	- 668.5
		6	0.0087	111	1:2:2	12,759	134940	23.1	- 658.3
B	SNM190305-1-2	2	0.0144	97	1:4:4	6736	574780	21.1	- 240.9
B	SNM190305-2-3	4	0.0144	93	1:2.9:2.9	6458	186470	21.1	- 305.6
		5	0.0144	86	1:6.7:6.7	5972	853700	20.8	- 178.8
		6	0.0144	99	1:2.5:2.5	6875	122140	21.3	- 332.1
L	SNM19_17	2	0.0144	152	1:2.5:2.5	10,556	349000	21.9	- 366.5
		4	0.0144	180	1:6.7:6.7	12,500	1792490	21.5	- 167.1
		6	0.0144	195	1:2.5:2.5	13,542	258300	22.4	- 423.3
L	SNM190420A-1E	3	0.0144	126	1:2.5:2.5	8750	191380	21.4	- 322.1
		4	0.0144	159	1:4:4	11,042	586090	21.6	- 248.7
L	SNM19051302-2-22	2	0.0144	139	1:5:5	9653	1566960	21.4	- 227.3

2000; Cashman and Blundy 2000). The shape of the CSD curve (slope and  $y$ -axis intercept) indicates the relative proportions of crystal growth and nucleation activity in the magma (Cashman 1992; Hammer et al. 1999, 2000). Textural data can be used to model the dynamics of the 2017–2018 Shinmoedake eruption; we detail our model based on pumice characteristics in the following section.

The initial pumice (Sample P1) showed low density and high vesicularity, with the highest measured plagioclase number density ( $1.9 \times 10^6/\text{mm}^3$ , Fig. 9) and a steep CSD slope for microlites smaller than 0.01 mm. The P1-type pumice likely formed in high undercooling conditions that allowed both active nucleation and crystal growth. However, fast ascent and limited degassing resulted in weak explosive eruptions during the early phase in March 2018. Sample P2 showed high vesicularity, the lowest plagioclase number density ( $1.2 \times 10^5/\text{mm}^3$ ), the highest CSD  $y$ -axis intercept value (approximately  $23/\text{mm}^4$ ), and the steepest CSD slope for small microlites (3D long-axis diameters shorter than 0.01 mm). These characteristics suggest that nucleation was dominant in Sample P2 and that crystal growth was likely inhibited by strong undercooling.

Sample L had higher groundmass crystallinity (59.2%) than Sample P1 (36.5%) but a lower plagioclase number

density ( $7.9 \times 10^5/\text{mm}^3$ ), likely because crystal growth dominated nucleation, although this is unclear from the CSD curves (Fig. 10). Results for B (Figs. 9, 10) yielded comparable but slightly lower values than for L for the groundmass crystallinity (52.5%), plagioclase number density ( $4.3 \times 10^5/\text{mm}^3$ ), and  $y$ -axis intercept ( $20.8\text{--}21.3/\text{mm}^4$ ). These results suggest that nucleation was inhibited in Sample B. Because B showed higher crystallinity but lower plagioclase number density compared with P1 (Fig. 9), the B magma likely evolved at slower cooling rates than the P1 magma.

The large  $y$ -axis intercept of the CSD curve for Sample P2 likely derives from enhanced undercooling induced by temporary stalling and equilibration of the magma. Liquidus temperatures increase with decreasing pressure and water (H<sub>2</sub>O) abundance, resulting in stronger undercooling at shallower depths during the isothermal ascent of the magma (Hammer et al. 1999, 2000; Cashman and Blundy 2000; Brugger and Hammer 2010). Consequently, stronger undercooling during stalling at shallow depths results in higher nucleation rates, producing the abundant small microlites observed in Sample P2. However, the lower plagioclase number density in P2 indicates that the shallow-depth stalling time was short; consequently, crystal growth was inhibited. Sample P2



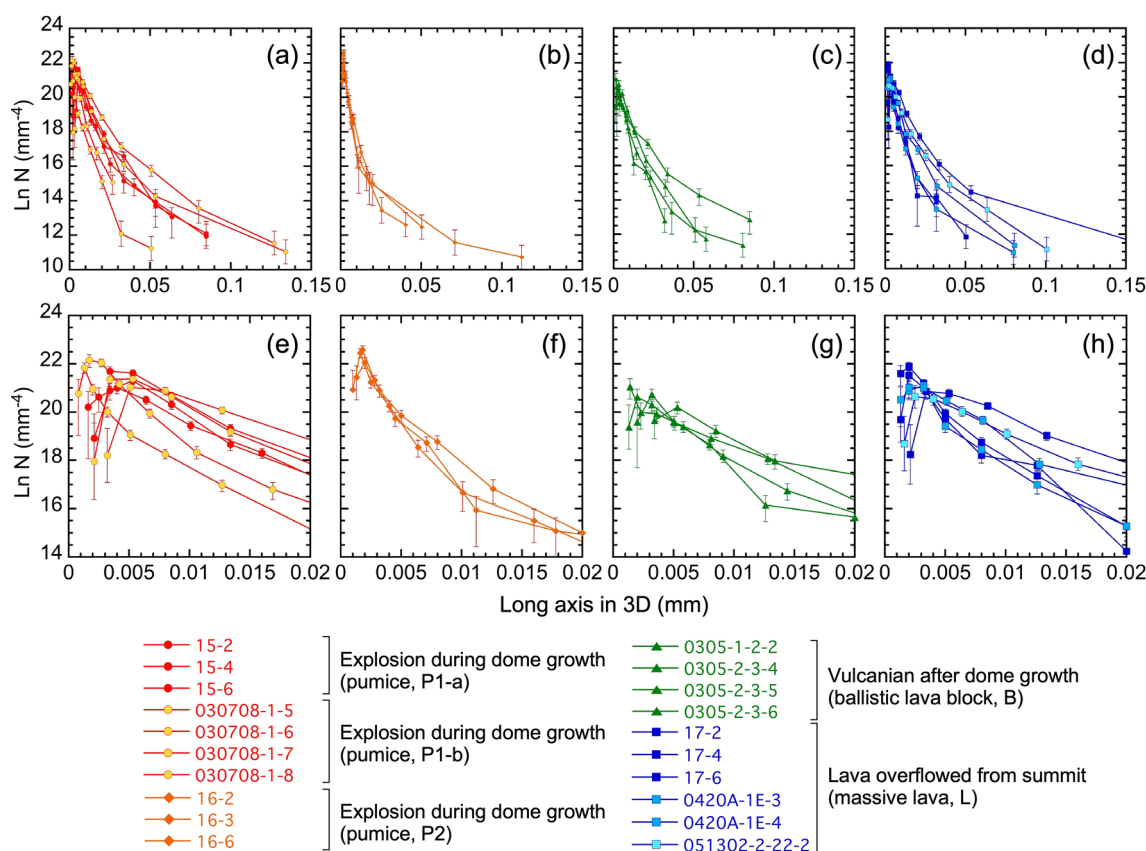


**Fig. 10** Calculated crystal size distribution (CSD) curves for sample types (a, e) P1, (b, f) P2, (c, g) B, and (d, h) L from the March 2018 Shinmoedake eruption and for crystals with 3D long-axis diameters shorter than (a–d) 0.15 mm and (e–h) 0.02 mm. Results for different P1-type samples are indicated separately in panel (e)

was likely produced during the explosions on 8–9 March 2018, which may have been caused by gas accumulation and/or rising gas-rich magma in the shallow conduit, as observed in the inflation of the lava dome surface immediately prior to the explosions. Although it cannot be determined whether P2 originated from such rising magma itself or from deeper sources, it is reasonable to consider that the P2 magma erupted explosively to the surface without experiencing a long stalling. Conversely, the higher groundmass crystallinity and plagioclase number density in samples B and L indicate longer stalling times at shallow depths, increasing the possibility of crystallization.

The hybrid explosive–effusive activity phase, with explosions and lava effusion forming P1 and L, respectively, suggests similar ascent paths for P1 and L. This is confirmed by their comparable CSD slopes and *y*-axis intercepts, accompanied by the stronger cooling and complete emplacement enhanced crystal growth in L. If P1 and L were erupted simultaneously, the ascending magma should exhibit velocity and vesicularity

differences across a horizontal conduit section with, for example, high velocity and vesicularity at the center and lower values at the margin. A similar conduit profile was proposed by Matsumoto and Geshi (2021) from their analysis of volcanic ash erupted during a phase of hybrid activity, which contained both vesicular and dense particles. In our study, Sample P1 is crystallized similarly to Sample P2 (Fig. 9) but has a smaller *y*-axis intercept and slope (Fig. 10), likely because of a slower magma ascent rate in the eruption that ejected Sample P1. Indeed, P1 pumice was produced in the early phases of lava effusion and likely corresponded to a weaker magma discharge.

Although samples L and B likely followed similar ascent paths, their microtextures differ. This was likely caused by differences in their surface cooling processes. Sample L cooled gradually while lava overflowed from the summit crater rim and was emplaced, whereas Sample B was ejected and cooled rapidly before solidification. This result is confirmed by consistently lower estimates of the crystallinity, plagioclase number density, and *y*-axis intercept for B than for L.

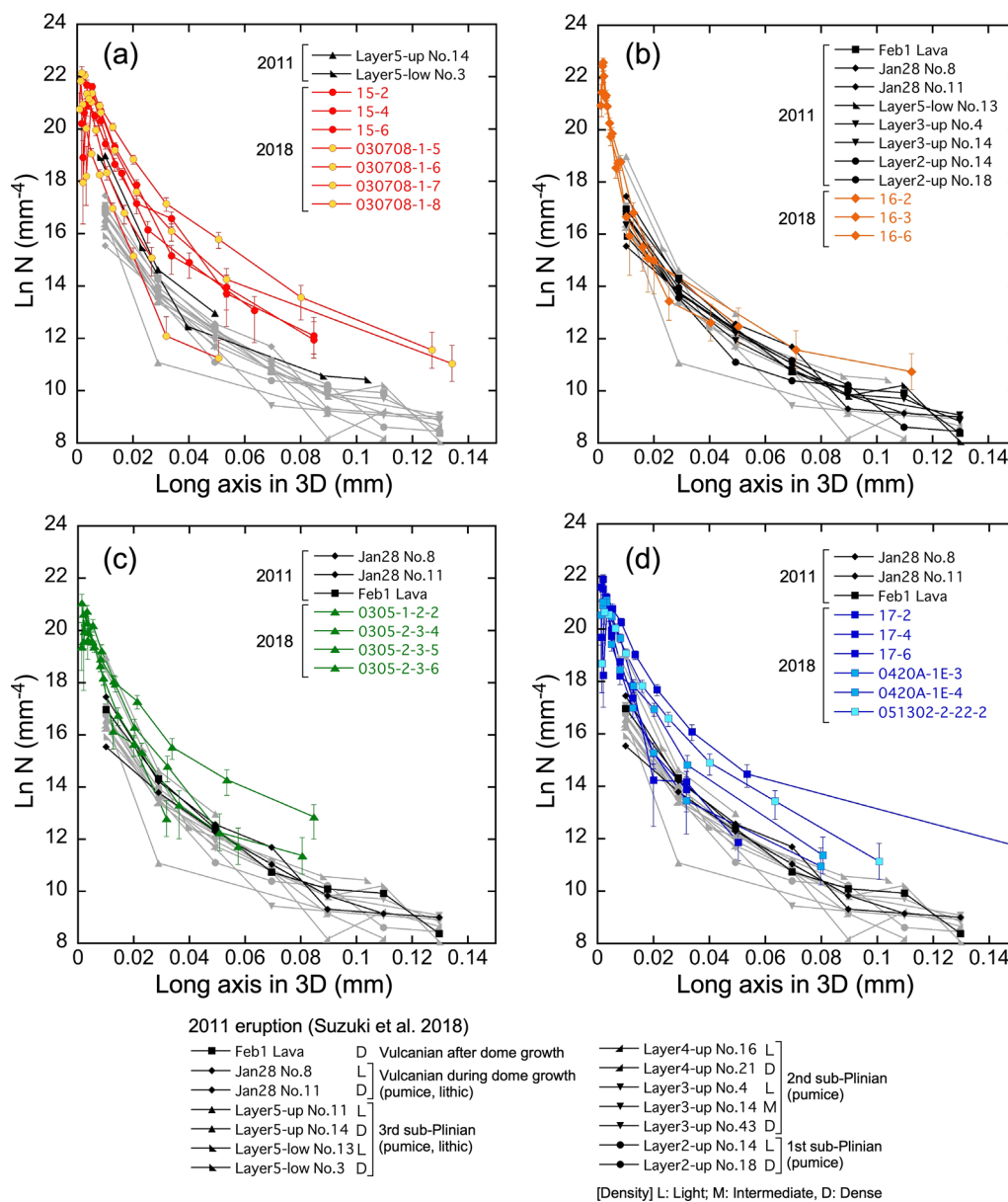


**Fig. 11** Reproduction of panels (a–d) of Fig. 10 for the March 2018 Shinmoedake eruptions but with the results for the 2011 eruption (Suzuki et al. 2018) also indicated (gray/black CSD curves). The CSD curves of the 2011 samples particularly important for comparison with our analysis of the March 2018 activities are shown in black

### Comparison with the 2011 subplinian and Vulcanian eruptions

The erupted masses or volumes during the 2018 explosive–effusive eruption phase were estimated to be on the order of  $10^8$  kg for tephra (The Joint Research Team for ash fall from Shinmoedake 2018) and  $1.5 \times 10^7$  m<sup>3</sup> for lava (Asia Air Survey et al. 2018). The corresponding results for the 2011 eruption were  $2\text{--}4 \times 10^7$  m<sup>3</sup> ( $2.5\text{--}5.0 \times 10^{10}$  kg) for tephra ejected by subplinian explosions and  $1.2\text{--}1.5 \times 10^7$  m<sup>3</sup> for lava (Kozono et al. 2013; Maeno

et al. 2014). The global eruptive volume was smaller in 2018 than in 2011 because of the absence of subplinian tephra; however, the estimated lava volumes were comparable. The average magma discharge rate during the lava effusion phase of the 2018 eruptions was estimated at approximately 72 m<sup>3</sup>/s (approximately  $1.8 \times 10^5$  kg/s) from the volume change and duration of crustal deformation (National Research Institute for Earth Science and Disaster Resilience 2018). In 2011, the magma discharge rate during lava effusion was estimated at 70–87

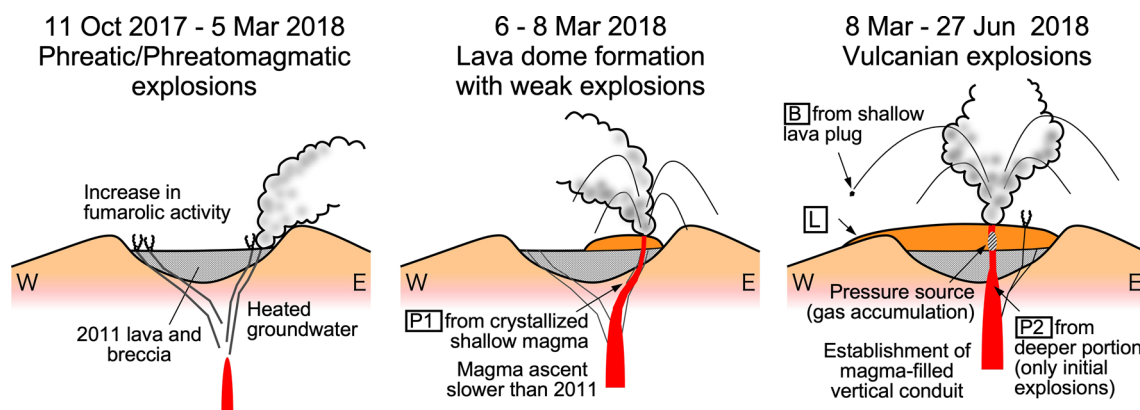


**Fig. 12** Model of the eruption style transition from October 2017 to June 2018 derived from our analysis of the surface phenomena and eruptive products

$\text{m}^3/\text{s}$  (approximately  $1.8 \times 10^5$ – $2.2 \times 10^5$   $\text{kg}/\text{s}$ ) (Kozono et al. 2013), although the discharge rate during the subplinian phase was  $1.0$ – $2.0 \times 10^6$   $\text{kg}/\text{s}$  (Maeno et al. 2014). Therefore, the 2011 and 2018 eruptions were very similar, except for the 2011 subplinian explosions and the associated tephra ejection.

Although the 2018 eruptions were primarily characterized by lava effusion, the eruption on 6–7 March was accompanied by explosions that formed a plume with a height of more than 1 km. Pumice clasts were ejected during a phase of hybrid activity; however, there was no subplinian style eruption, contrary to 2011. Moreover, the 2018 P2-type pumice was characterized by similar vesicularity, crystallinity, and CSD as that ejected from the 2011 subplinian eruptions. These eruptive phenomena and products indicate that the 2018 eruption conditions were nearly those of subplinian fragmentation. This assumption is supported by the empirical relationship between the magma discharge rate and the eruption style, which defines the boundary between the subplinian and lava dome-forming eruption styles as transitional (Cashman 2004; Gonnermann and Manga 2013) and potentially influenced by small differences in the magma discharge rate (Kozono et al. 2013).

Groundmass textures of the 2018 products were further compared with those from 2011 (Suzuki et al. 2018). The CSD curves for representative samples from both eruptions are shown in Fig. 11. The dependence of the density and groundmass crystallinity on the plagioclase number density (Fig. 9, left and right panels, respectively) shows that Sample P2 was similar to samples from the third subplinian eruption of 2011 (“Layer 5-up” and “Layer 5-low,” 27 January 2011) and Sample B was comparable to samples from the Vulcanian explosions on 1 February 2011 (“Feb 1 lava”). Conversely, the high plagioclase

number density of Sample P1 was not observed in any of the 2011 samples.

Suzuki et al. (2018) hypothesized that, during the 2011 eruption, high-density and high-crystallinity (or high plagioclase number density) pumice experienced strong undercooling, which promoted crystal nucleation as it slowly ascended in the upper conduit during the quiescent period, while low-density and low-crystallinity (or low plagioclase number density) pumice ascended at high velocity during the subplinian explosions. Similarly, we assume that P1 slowly ascended in the upper conduit prior to the start of the 2018 magmatic eruption, whereas P2 was produced from magma that ascended rapidly from the deeper conduit in response to intense Vulcanian-style explosions (Fig. 12). The extreme styles of Vulcanian explosions can be defined as a discrete, short-lived explosion similar to a firing cannon (e.g., McBirney 1973; Fagents and Wilson 1993) versus a markedly longer, sustained explosion (e.g., Clarke et al. 2015). In the latter case, not only the dense surface cap rock but also vesiculated magma erupts from depths of several hundreds of meters in the deeper conduit (e.g., Soufriere Hills, Giachetti et al. 2010; Burgisser et al. 2011). Although the depth of the P2 magma is not well determined as discussed above, its textural characteristics, similar to the 2011 subplinian pumice (Fig. 11b), indicate that P2 experienced a relatively high discharge rate with limited stalling. Therefore, we believe that P2 was produced during a sustained-type Vulcanian explosion caused by deep-conduit magma. Production of such pumice is generally limited to the early phase of lava dome growth. This strengthens the hypothesis that P2 was produced under high-magma supply rate conditions rather than during the static or slow phases following lava effusion. Subsequently, explosive activity was restricted to shallow gas

accumulation and the disruption of the surface cap rock, thereby primarily producing B-type material in the shallow part of the conduit, as observed during the discrete, short-lived explosion on 14 March 2018 (Fig. 6).

Finally, the 2011 eruption that formed the “Layer 5” material, the sample type with the highest crystal number density among the 2011 eruptive products (Fig. 11a), likely occurred under predominant nucleation conditions and was followed by lava accumulation in the summit crater. This is similar to the initial phase of the March 2018 eruption that produced P1 which has a high plagioclase number density like the “Layer 5”. However, Sample P1 is more vesiculated than the “Layer 5” material. Such pumice, not observed in 2011, might characterize a type of magma ascent for which the mass discharge rate is sufficiently high to cause explosions but does not induce subplinian eruptions.

## Conclusions

In October 2017, phreatic and phreatomagmatic explosions occurred at the eastern edge of the summit crater of the Shinmoedake volcano in Kirishima, Japan. A phase of hybrid activities occurred in March 2018. This phase was characterized by simultaneous explosions and lava flows and transitioned toward intermittent Vulcanian-style explosions at the center of the newly formed lava dome. The whole-rock chemical compositions of the volcanic ash changed with time and became similar to those of the lava and pumice ejected during the main eruption (March 2018). Crustal deformation data indicate that magma accumulated at depth and that small-scale eruptions from October 2017 to early March 2018 were likely caused by the activation or pressurization of a shallow hydrothermal system.

Variability in the chemical and textural features of the 2018 eruptive products (P1, P2, B, and L) reflects distinct cooling and magma ascent processes. The initial pumice P1, erupted during the formation of the lava dome, showed high crystallinity and the highest plagioclase number density. Conversely, pumice P2, from the initial Vulcanian explosions on 8–9 March 2018, had the lowest plagioclase number density and its CSD curve had the highest *y*-axis intercept. The characteristics of Sample P2 were similar to those of subplinian pumice from the previous Shinmoedake eruptions in 2011. The characteristics of samples B and L were comparable to those of Vulcanian ballistics from the 2011 eruptions. Sample P2 likely experienced a high discharge rate caused by deeper conduit magma. Contrary to P2, B, and L, P1-type material was not observed in 2011. Therefore, such pumice might be exclusive to hybrid eruptions that include

small-scale explosions and lava dome formation with low magma discharge. We believe that the transitions in the activities and eruption styles observed during the 2017–2018 Shinmoedake eruptions, and their temporal evolution, are strongly influenced by the ascent rate of andesitic magma and the geological structure beneath the summit crater. We suggest that a similar mechanism could cause activity transition and eruption style changes in other andesitic volcanoes.

## Abbreviations

CSD	Crystal size distribution
EPMA	Electron probe microanalyzer
ERI	Earthquake Research Institute, The University of Tokyo
GSI	Geospatial Information Authority of Japan
JMA	Japan Meteorological Agency

## Acknowledgements

We thank JMA, GSI, and Asia Air Survey Co., Ltd. for providing their remote observation data and analysis results. We also thank JMA, the city of Kirishima, and the Kagoshima Regional Forest Office for supporting our field surveys. Constructive comments from Giachetti T and Pioli L were helpful in improving the manuscript.

## Author contributions

SS and FM conceptualized the study and oversaw data collection and analysis. FM wrote the first draft of the manuscript. SY provided the previous dataset and contributed to the result interpretation. SS, NH, and AY conducted the X-ray fluorescence spectrometry and EPMA analyses. FM, TK, and SN conducted aerial surveys and made geological interpretations. SS, FM, YI, and SN conducted geological investigations and rock sampling. All authors discussed the eruption process, contributed to manuscript revisions, and approved this submission. All authors read and approved the final manuscript.

## Funding

This research was supported by a Grant-in-Aid for Scientific Research (Number 20KK0075) from the Ministry of Education, Culture, Sports, Science and Technology of Japan (MEXT) and by the MEXT Earthquake and Volcano Hazards Observation and Research Program (Projects ERI03 and ERI17).

## Availability of data and materials

All data analyzed and discussed during this study are available from the corresponding author upon reasonable request.

## Declarations

### Ethics approval and consent to participate

Not applicable.

### Consent for publication

Not applicable.

### Competing interests

The authors declare that they have no competing interests.

## Author details

<sup>1</sup>Earthquake Research Institute, The University of Tokyo, 1-1-1 Yayoi, Bunkyo-ku, Tokyo 113-0032, Japan. <sup>2</sup>Tera Technology, Inc, Ikebukuro East Bldg., Higashi Ikebukuro 3-4-3, Toshima-ku, Tokyo 170-0013, Japan. <sup>3</sup>Waseda University, 1-6-1 Nishi-Waseda, Shinjuku-ku, Tokyo 169-8050, Japan. <sup>4</sup>Department of Earth and Planetary Science, The University of Tokyo, 7-3-1 Hongo, Bunkyo-ku, Tokyo 113-0033, Japan. <sup>5</sup>National Research Institute for Earth Science and Disaster Resilience, 3-1 Tennodai, Tsukuba 305-0006, Japan.

Received: 21 October 2022 Accepted: 25 April 2023  
Published online: 11 May 2023

## References

- Asia Air Survey, Geological Survey of Japan, Earthquake Research Institute Univ. Tokyo, Kumamoto Univ (2018) On the volume change of lava associated with the 2018 eruption of Shinmoedake. Rep Coord Comm Predict Volcan Erupt 141:189–194
- Brugger CR, Hammer JE (2010) Crystallization kinetics in continuous decompression experiments: implications for interpreting natural magma ascent processes. *J Petrol* 51:1941–1965
- Burgisser A, Arbaret L, Druitt T, Giachetti T (2011) Pre-explosive conduit conditions of the 1997 Vulcanian explosions at Soufrière Hills Volcano, Montserrat: II. overpressure and depth distributions. *J Volcanol Geotherm Res* 199:193–205. <https://doi.org/10.1016/j.jvolgeoes.2010.11.014>
- Cashman KV (1992) Groundmass crystallization of Mount St. Helens dacite, 1980–1986: a tool for interpreting shallow magmatic processes. *Contrib Mineral Petrol* 109:431–449
- Cashman KV (2004) Volatile controls on magma ascent and eruption, in the state of the planet: frontiers and challenges in geophysics Geophy. Monogr Ser 150 edited by Sparks RSJ. Hawkesworth. CJ 109–124. <https://doi.org/10.1029/150GM10>
- Cashman KV, Blundy JD (2000) Degassing and crystallization of ascending andesite and dacite. *Phil Trans Royal Soc London Ser A* 358:1487–1513
- Cashman KV, Sparks RSJ (2013) How volcanoes work: a 25 year perspective. *Bull Geol Soc Am Bull* 125:664–690
- Cassidy M, Manga M, Cashman K, Bachmann O (2018) Controls on explosive-effusive volcanic eruption styles. *Nature Comm* 9:2839
- Clarke AB, Esposti Ongaro T, Belousov A (2015) Vulcanian eruptions, in *The Encyclopedia of Volcanoes* (Second Edition) edited by Sigurdsson H et al. Academic Press, Cambridge
- Earthquake Research Institute Univ Tokyo (2018) Crater conditions and fumarolic activity of the 2018 eruption of Shinmoedake, Kirishima Volcano Group. Rep Coord Comm Predict Volcan Erupt 141:105–110
- Fagents SA, Wilson L (1993) Explosive volcanic eruptions VI: the ranges of pyroclasts ejected in transient volcanic eruptions. *Geophys J Int* 113:359–370
- Geospatial Information Authority of Japan (2018) Response to the 2018 Shinmoedake eruption, Kirishima, <https://www.gsi.go.jp/BOUSAI/h30kirishima-index.htm>. Accessed on 20 December 2021.
- Giachetti T, Druitt TH, Burgisser A, Arbaret L, Galven C (2010) Bubble nucleation, growth and coalescence during the 1997 Vulcanian explosions of Soufrière Hills Volcano, Montserrat. *J Volcanol Geotherm Res* 193:215–231
- Gonnermann HM, Manga M (2013) Dynamics of magma ascent in the volcanic conduit, in *Modeling volcanic processes* edited by. Cambridge University Press, Cambridge
- Hammer JE, Cashman KV, Hoblitt RP, Newman S (1999) Degassing and micro-lite crystallization during pre-climactic events of the 1991 eruption of Mt. Pinatubo Philippines. *Bull Volcanol* 60:355–380
- Hammer JE, Cashman KV, Voight B (2000) Magmatic processes revealed by textural and compositional trends in Merapi dome lavas. *J Volcanol Geotherm Res* 100:165–192
- Higgins MD (2000) Measurement of crystal size distributions. *Am Mineral* 85:1105–1116
- Imura R, Kobayashi T (1991) Eruptions of Shinmoedake Volcano, Kirishima Volcano Group, in the last 300 years. *Bull Volcanol Soc Jap* 36:135–145
- Imura R, Kobayashi T (2001) Geological map of Kirishima volcano. *Geol Survey Japan Geol Map Volcan* 11:1
- Japan Meteorological Agency (2018) Kirishima Volcano. Rep Coord Comm Predict Volcan Erupt 140:3–65
- Joseph EP, Camejo-Harry M, Christopher T, Contreras-Arratia R, Edwards S, Graham O, Johnson M, Juman A, Latchman JL, Lynch L, Miller VL, Papadopoulos I, Pascal K, Robertson R, Ryan GA, Stinton A, Grandin R, Hamling I, Jo M-J, Barclay J, Cole P, Davies BV, Sparks RSJ (2022) Responding to eruptive transitions during the 2020–2021 eruption of La Soufrière volcano. *St Vincent Nature Comm* 13:4129. <https://doi.org/10.1038/s41467-022-31901-4>
- Kozono T, Ueda H, Ozawa T, Koyaguchi T, Fujita E, Tomiya A, Suzuki YJ (2013) Magma discharge variations during the 2011 eruptions of Shinmoedake volcano, Japan, revealed by geodetic and satellite observations. *Bull Volcanol* 75:695–707
- Maeno F, Nakada S, Nagai M, Kozono T (2013) Ballistic ejecta and eruption condition of the vulcanian explosion at Shinmoedake volcano, Kirishima, Japan on 1 Feb, 2011. *Earth Planet Space* 65:609–621. <https://doi.org/10.5047/eps.2013.03.004>
- Maeno F, Nagai M, Nakada S, Burden R, Engwell S, Suzuki Y, Kaneko T (2014) Constraining tephra dispersion and deposition from three subplinian explosions at Shinmoedake volcano, Kyushu, Japan, 2011. *Bull Volcanol* 76:823. <https://doi.org/10.1007/s00445-014-0823-9>
- Matsumoto K, Geshi N (2021) Shallow crystallization of eruptive magma inferred from volcanic ash microtextures: a case study of the 2018 eruption of Shinmoedake volcano. *Japan Bull Volcanol* 83:31. <https://doi.org/10.1007/s00445-021-01451-6>
- McBirney AR (1973) Factors governing the intensity of explosive andesitic eruptions. *Bull Volcanol* 37:443–453
- Miyabuchi Y, Hanada D, Niimi H, Kobayashi T (2013) Stratigraphy, grain-size and component characteristics of the 2011 Shinmoedake eruption deposits, Kirishima Volcano, Japan. *J Volcanol Geotherm Res* 258:31–46
- Mujin M, Nakamura M (2014) A nanolite record of eruption style transition. *Geology* 42(7):661–614
- Mujin M, Nakamura M, Miyake A (2017) Eruption style and crystal size distributions: crystallization of groundmass nanolites in the 2011 Shinmoedake eruption. *Am Mineral* 102:2367–2380
- Nakada S, Nagai M, Kaneko T, Suzuki Y, Maeno F (2013) The outline of the 2011 eruption at Shinmoedake (Kirishima) Japan. *Earth Planet Space* 65:475–488. <https://doi.org/10.5047/eps.2013.03.016>
- Nakada S, Zaennudin A, Yoshimoto M, Maeno F, Suzuki Y, Hokanishi N, Sasaki H, Iguchi M, Ohkura T, Gunawan H, Triastuty H (2019) Growth process of the lava dome/flow complex at Sinabung Volcano during 2013–2016. *J Volcanol Geotherm Res* 382:120–136. <https://doi.org/10.1016/j.jvolgeoes.2017.06.012>
- National Research Institute for Earth Science and Disaster Resilience (2018) A change of lava in the Shinmoedake crater estimated by SAR. Rep Coord Comm Predict Volcan Erupt 141:159–163
- Oikawa T, Maeno F, Miyabuchi Y, Nagai M, Shimano T, Furukawa R, Naruo H, Nakada S, Ikenaga Y, Miwa T, Iriyama Y, Nakano S, Ishizuka Y, Tajima Y (2018) Masses of tephra fall deposit from the 2017 Shinmoedake eruption, Kirishima Volcanoes, Kyushu, Japan. Japan Geoscience Union Meeting 2018 SVC41-P39 (in Japanese)
- Pallister JS, Schneider DJ, Griswold JP, Keeler RH, Burton WC, Noyles C, Newhall CG, Ratdomopurbo A (2013) Merapi 2010 eruption—chronology and extrusion rates monitored with satellite radar and used in eruption forecasting. *J Volcanol Geotherm Res* 261:144–152
- Preece K, Barclay J, Gertisser R, Herd RA (2013) Textural and micro-petrological variations in the eruptive products of the 2006 dome-forming eruption of Merapi volcano, Indonesia: implications for sub-surface processes. *J Volcanol Geotherm Res* 261:98–120
- Shea T, Houghton B, Gurioli L, Cashman KV, Hammer JE, Hobden BJ (2010) Textural studies of vesicles in volcanic rocks: an integrated methodology. *J Volcanol Geotherm Res* 190:271–289
- Suzuki Y, Yasuda A, Hokanishi N, Kaneko T, Nakada S, Fujii T (2013a) Syneruptive deep magma transfer and shallow magma remobilization during the 2011 eruption of Shinmoedake, Japan: constraints from melt inclusions and phase equilibria experiments. *J Volcanol Geotherm Res* 257:184–204
- Suzuki Y, Nagai M, Maeno F, Yasuda A, Hokanishi N, Shimano T, Ichihara M, Kaneko T, Nakada S (2013b) Precursory activity and evolution of the 2011 eruption of Shinmoedake in Kirishima volcano—insights from ash samples. *Earth Planet Space* 65:591–607. <https://doi.org/10.5047/eps.2013.02.004>
- Suzuki Y, Maeno F, Nagai M, Shibutani H, Shimizu S, Nakada S (2018) Conduit processes during the climactic phase of the Shinmoedake 2011 eruption (Japan): insights into intermittent explosive activity and transition in eruption style of andesitic magma. *J Volcanol Geotherm Res* 358:87–104
- Taddeucci J, Pompilio M, Scarlato P (2004) Conduit processes during the July–August 2001 explosive activity of Mt. Etna (Italy): inferences from glass chemistry and crystal size distribution of ash particles. *J Volcanol Geotherm Res* 137:33–54
- The Joint Research Team for ash fall from Shinmoedake (2018) Tephra volumes from the March–May 2018 eruptions at Shinmoedake. Rep Coord Comm Predict Volcan Erupt 141:195–196

- Wadge G, Voight B, Sparks RSJ, Cole PD, Loughlin SC, Robertson REA. 2014 Chapter 1. An overview of the eruption of Soufrière Hills Volcano Montserrat from. *Geol Soc London Mem.* 39 1–49
- Yamada T, Ueda H, Mori T, Tanada T (2019) Tracing volcanic activity chronology from a multiparameter dataset at Shinmoedake volcano (Kirishima), Japan. *J Disaster Res* 14:687–700

### **Publisher's Note**

Springer Nature remains neutral with regard to jurisdictional claims in published maps and institutional affiliations.

**Submit your manuscript to a SpringerOpen<sup>®</sup> journal and benefit from:**

- ▶ Convenient online submission
- ▶ Rigorous peer review
- ▶ Open access: articles freely available online
- ▶ High visibility within the field
- ▶ Retaining the copyright to your article

---

Submit your next manuscript at ▶ [springeropen.com](https://www.springeropen.com)

---